CHAPTER 5: RALOXIFENE

5.1. Introduction:

Raloxifene hydrochloride (RLX) has its potential application in the treatment of osteoporosis and cancer especially in breast cancer. It is a second generation selective estrogen receptor modulator (SERM) with established estrogenic activity which make it a potential candidate for use in the therapy of osteoporosis (1, 2). RLX comes under the category of Biopharmaceutical Classification System (BCS) class II. The oral bioavailability of the RLX is limited to only 2%, which is accredited to extensive first pass metabolism (FPM) of RLX. Roughly 60% of the oral RLX dose undergoes FPM. The poor aqueous solubility along with significant FPM together contributes towards its lower bioavailability (3, 4).

Formulating a nano level delivery system may significantly decrease the FPM of drugs like RLX and significantly enhance its dissolution rate profile and bioavailability as well (5). In the present work we have studied the influence of 2D and 3D pore structure along with effect of surface functionalization on the dissolution and bioavailability profile of RLX. Surface decoration using amine moiety may give a controlled release of the cargo from the pores. In this investigation, we concluded from the comprehensive study that 3D cubic interior gives a promising outcome for bioavailability increment. Besides, the pristine MSN molecules demonstrated a burst release within a few minutes of oral administration of formulated nanoparticles whereas, the amine coating on the bare nanoparticles exhibited a significant hindrance in the release of RLX which is due to the presence of alkyl amine group over the surface. This would be beneficial in formulating MSNs based controlled drug delivery systems.

Stimuli responsive smart polymeric drug delivery system is gaining attention now a days, especially in tumor targeting. In particular, external surface decoration of mesoporous by different stimuli responsive is in the limelight now days due to its biocompatibility, large surface area, uniform and tunable pore size, noteworthy loading efficiency with zero premature release *etc*. Temperature, pH, redox, *etc* are the various stimuli by which one can focus the drug delivery to target site only. From all these options available, pH is the most easiest and feasible way to achieve stimuli responsive drug delivery (6, 7). Chitosan is the commonly used polysaccharide in the drug delivery system due to its non-toxic, biocompatible and bio degradative nature. The presence of abundant amine group on the outer surface make chitosan freely soluble in the pH range of 1 to 11. Moreover, being a polysaccharide, it also controls the release of the drug. Additionally, the unique feature of swelling at lower pH makes chitosan a favourable candidate to formulate a pH responsive drug delivery system (8, 9). On the other

hand, ligand mediated targeting can selectively bind to a specific receptor overexpressed in cancer and will direct the release to cancer cells only. Folic acid (FA) is one of the most widely used ligand as it is widely available, inexpensive, water soluble and stable vitamin, zero adverse effect to healthy cells and low immunogenic. It has an affinity towards and gets selectively bound to the folate receptors. These receptors are overexpressed in epithelial malignancies like colorectal, ovarian and breast cancer compared to normal cells. Surface decoration of MSNs with folic acid ligand could be applied in the formulation of receptor based active targeting drug delivery system. Further, the decoration of MSNs with chitosan as well as folic acid may make it a perfect drug delivery system possessing a dual characteristic i.e. stimuli responsive as well as receptor based nano drug delivery system (10).

In the present chapter, how MSNs improve the *in vitro* release profile and *in vivo* pharmacokinetics behaviour of RLX is discussed in details. Further, the application of chitosan and folic acid to engineer the pH triggered and receptor-based drug release has also been deliberated in depth.

5.2. Materials and methods:

5.2.1. Chemicals and reagents:

An active pharmaceutical ingredient (API) Raloxifene hydrochloride (RLX; ≥99%) was acquired as a sample gratis from Zydus research centre, Gujarat, India. Other ingredients like fumed silica, tetra methyl ammonium hydroxide pentahydrate (TMAOH; ≥98%), tetraethyl orthosilicate (TEOS; ≥99%), cetyl trimethyl ammonium bromide (CTAB; ≥99%), (3-aminopropyl) triethoxysilane (APTES; ≥99%) utilized in the synthesis of MSNs were procured from Sigma Aldrich (USA). Deionized water was used in the synthesis of MSNs.

HPLC grade methanol (MeOH) and acetonitrile (ACN) were procured from Fisher Scientific (Vadodara, Gujarat) to carry out chromatographic analysis. Different reagents utilized during dissolution and diffusion study like hydrochloric acid (HCl), potassium dihydrogen phosphate, acetic acid, ammonium formate, formic acid, polysorbate-80, hydrochloric acid, sodium acetate trihydrate, acetic acid, monobasic potassium phosphate and sodium chloride were acquired from Loba Chemie (Mumbai, Maharashtra). Unless otherwise stated, all chemicals were utilized as received and reagents were of analytical grade.

The cytotoxicity study was carried out on *in vitro* model of epithelial cells *i.e.* Caco-2 (for oral formulation) and MCF-7 (for parenteral formulation) which were procured from the National Centre for Cell Science (NCCS, Pune, India) and the cells were cultured in T-25 cm^2 tissue culture flask supplemented with Dulbecco's modified eagle medium (DMEM) media supplemented with 0.1% penicillin and streptomycin solution and 20% and 10% foetal bovine serum (FBS) for Caco-2 and MCF-7 cells respectively. The culture medium was replaced every alternative day. Cell culture grade dimethyl sulphoxide (DMSO ≥99%) and other culture solutions mentioned before were procured from Himedia laboratories. The 3– (4, 5-Dimethylthiazol-2-yl)-2, 5-diphenyltetrazolium bromide (MTT) dye was purchased from Sigma Aldrich (USA). Fluorescein isothiocyanate (FITC) and 4,6-Diamidino-2-Phenylindole Dihydrochloride (DAPI) were purchased from SRL chemicals (Mumbai). Various well plates and other materials used in the cell line study were purchased from HI media Laboratories.

Female Swiss albino mice (body weight, 20 ± 2 g) were supplied by Zydus Cadila healthcare Ltd, Gujarat, India. All the animal experiments performed in accordance with the protocols approved by the Institutional animal ethics committee (IEAC) guidelines having protocol number MSU/IAEC/2017-18/1725. The mice were acclimatized to the laboratory environment for a week with free water and food access before conducting the actual experiment.

5.2.2. Synthesis of MSN-41 and MSN-48 types of Nanocarriers:

5.2.2.1. Synthesis of MCM-41:

The MCM-41 synthesis was carried out as per the literature method with few modifications (11). Briefly, a thick slurry having a composition of SiO_2: 0.27 CTAB: 0.19 TMAOH: 40 H_2O was formulated and given the hydrothermal treatment at 373K for 2 days in the Teflon coated autoclave. This procedure was followed by the successive filtration, washing and drying step. Subsequently, the dried product was calcined in a muffle furnace at 823K for 5.5h for the purpose of a template (CTAB) removal. The collected final product was labelled as MCM-41.

5.2.2.2. Synthesis of MCM-48:

The MCM-48 synthesis was done as per the literature reported method (12). The gel mixture having a molar composition of SiO_2: 0.23 NaOH: 0.55 CTAB: 11 H_2O was stirred for 1.5 h and hydrothermal treatment was given in the Teflon lined autoclave at 283K for 72 h. Eventually, the product was recovered by filtration, washed thoroughly with plenty of water and dried overnight at 353K. Dried product was ignited at 573K initially for 2 h and at 823K for subsequent 8 h for total surfactant elimination and labelled as MCM-48 nanoparticles.

5.2.2.3. Synthesis of amine coated MCM-41 and MCM-48 nanoparticles:

The identical surface functionalization methodology was adopted for both MCM-41 as well as MCM-48. External grafting of amine moiety was secured following post synthetic grafting approach with few modifications (13, 14). Wherein, the dispersion of 0.1 grams MSNs in 25 mL toluene was treated with the 1.38 mL of APTES followed by refluxing the reaction mixture at 120 ºC for 24h. Subsequently, the obtained slurry was filtered and acquired material was labelled as MCM-NH_2-41 and MCM-NH_2-48.

5.2.2.4. Synthesis of chitosan coated MCM-41 and MCM-48 nanoparticles:

The chitosan grafting was conducted as per the reported method (7). Herein, chitosan solution of 0.5%w/v concentration was prepared in 3% acetic acid and stirred for 24 h at 600 rpm. On the other hand, the dispersion of pristine 10mg MCM-41 and MCM-48 in 5 mL MeOH was prepared individually and acidified in the pH range of 3.5-4.5 with the help of acetic acid. To this reaction mixture, 200µL of APTES was incorporated and stirred overnight. Eventually, the chitosan coated MCM-41 and MCM-48 nanoparticles were obtained following the addition of

5 mL chitosan solution to the above reaction mixtures separately. The final dispersions were centrifuged individually to 10000 rpm followed by thorough washing with the plenty of water. The collected material was freeze dried and labeled as MCM-CHITO-41 and MCM-CHITO-48 respectively.

5.2.2.5. Synthesis of folic acid-chitosan coated MCM-41 and MCM-48 nanoparticles:

The conjugation of folic acid and chitosan was performed as per the literature method (10). 1.12g folic acid and 0.4g EDC solution was mixed together in 40 mL anhydrous dimethyl formaldehyde and stirred continuously for 2 h at room temperature. Further this solution was added dropwise to a 0.5% w/v chitosan solution in 0.1M acetate buffer having pH 4.7. The mixture was stirred in dark for 12 h continuously. Later, the pH of the obtained mixture was adjusted to 9 by 1M NaOH. Subsequently the yellow precipitate was obtained by centrifugation at 2500 rpm. It was then dialyzed against PBS (pH 7.4) for 3 days and further against water. Lastly, folic acid-chitosan (FC) conjugates were isolated by lyophilization.

Now, the coating FC conjugates on MCM-41 and MCM-48 was carried out as follows. A mixture of 50 mg FC powder in 10 mL 3% acetic acid was stirred for 24 h to get a 0.5%w/v solution. 20 mg MSNs was dispersed in 10 mL methanol for 10 min. The pH was maintained in the range 3.5-4.5 by adding acetic acid. Next, 10 mL of FC solution was added to the aforementioned mixture and kept for stirring at room temperature for 24h. The FC coated MSNs were obtained by centrifugation at 10000 rpm. The yellow precipitate was separated from solution, washed with water and excess methanol and ultimately freeze-dried and the products were labelled as MCM-FC-41 and MCM-FC-48.

5.2.3. Drug loading inside the nanopores:

A novel immersion-solvent evaporation method was employed for encapsulation of RLX inside the mesopores (15). Briefly, highly concentrated methanolic RLX solution (5000 µg/mL) was prepared and MCM-41, MCM-NH_2-41, MCM-CHITO-41, MCM-FC-41 and MCM-48, MCM-NH_2-48, MCM-CHITO-48, MCM-FC-48 were dispersed individually to have 1:1.5 drug: carrier mass ratio. This dispersion was stirred vigorously and subsequently subjected to rotary evaporation to obtain dried RLX incorporated nanoparticles. The secured drug filled nanoparticles were termed as RLX-41, RLX-NH_2-41, RLX-CHITO-41, RLX-FC-41 and RLX-48, RLX-NH_2-48, RLX-CHITO-48, RLX-FC-48 respectively. %Drug loading and %entrapment efficiency was determined by UV-VIS spectrometry at 287 nm wavelength for RLX using below equations.

$$\%Entrapment\ Efficiency = \frac{Total\ weight\ of\ RLX\ present\ in\ nanoparticles}{Weight\ of\ RLX\ added\ initially} \times 100 \ldots\ldots\ldots\ldots\ldots\ldots 5.1$$

$$\%Loading\ Efficiency = \frac{Total\ weight\ of\ RLX\ present\ in\ nanoparticles}{Total\ weight\ of\ drug\ loaded\ nanoparticles} \times 100 \ldots\ldots\ldots\ldots\ldots 5.2$$

Further confirmation of %loading efficiency was done by TGA analysis. RLX loaded nanoparticles and RLX pure drug were subjected to thermal analysis up to 700 ºC with the heating rate of 5 ºC/min. % Loading results were divulged by plotting graphs of %weight loss versus temperature (ºC).

5.2.4. Solid state evaluation of pristine and functionalized MSNs:

The characterization of formulated RLX loaded nanoparticles as well as drug free nanoparticles were proceeded in the identical way. The synthesized MSNs were characterized for confirmation of the mesoporous skeleton integrity, for success of drug uptake, surface properties *etc* employing various characterization techniques.

5.2.4.1. FT-IR analysis:

Preliminary investigations for confirming the success of MCM-41 and MCM-48 synthesis was done through FTIR analysis using Bruker ALPHA-T FT-IR instrument where the spectra was scanned from 600 cm^{-1} to 4000 cm^{-1}. Furthermore, MCM-NH_2-41, MCM-CHITO-41, MCM-FC-41 and MCM-48, MCM-NH_2-48, MCM-CHITO-48, MCM-FC-48 were also evaluated by FTIR to affirm the success of surface grafting. Similarly, the FT-IR analysis for plain RLX, RLX-41, RLX-NH_2-41, RLX-CHITO-41, RLX-FC-41 and RLX-48, RLX-NH_2-48, RLX-CHITO-48, RLX-FC-48 was also perform in order to claim complete loading of the drug inside the pores.

5.2.4.2. DSC analysis:

The similar hypothesis of complete drug loading was confirmed by DSC analysis of RLX, RLX-41, RLX-NH_2-41, RLX-CHITO-41, RLX-FC-41 and RLX-48, RLX-NH_2-48, RLX-CHITO-48, RLX-FC-48 nanoparticles by thermal analysis up to 300 ºC on Shimadzu DSC60 model equipped with the TA 60-WS software with the scan rate of 10 ºC/min.

5.2.4.3. Wide angle x-ray diffraction (WXRD) analysis:

The speculation of complete drug loading was proved after wide angle x-ray diffraction (WXRD) analysis of RLX, RLX-41, RLX-NH_2-41, RLX-CHITO-41, RLX-FC-41 and RLX-48, RLX-NH_2-48, RLX-CHITO-48, RLX-FC-48 in the range of 10º to 40º on EMPYREAN, PANalytical model operated at 40 kV and 30 mA and equipped with Cu Ka radiation beam with the scanning rate of 0.03º/min on the same instrument.

5.2.4.4. Small angle x-ray diffraction (SXRD) analysis:

The detection of unique XRD peaks due to mesopore structure of MCM-41, MCM-NH_2-41, MCM-CHITO-41, MCM-FC-41 and MCM-48, MCM-NH_2-48, MCM-CHITO-48, MCM-FC-48 in small angle XRD were determined in the region of 1º to 10º on the similar instrument by keeping scan rates of 0.02º/min. SXRD was also performed for drug loaded nanoparticles *i.e.* RLX-41, RLX-NH_2-41, RLX-CHITO-41, RLX-FC-41 and RLX-48, RLX-NH_2-48, RLX-CHITO-48, RLX-FC-48 to confirm intactness of mesoporous integrity after drug encapsulation.

5.2.4.5. Dynamic light scattering (DLS) analysis:

The particle size and zeta potential for pristine and surface decorated nanoparticles *i.e.* MCM-41, MCM-NH_2-41, MCM-CHITO-41, MCM-FC-41 and MCM-48, MCM-NH_2-48, MCM-CHITO-48, MCM-FC-48 were ascertained from the dynamic light scattering (DLS) study operating MALVERN zeta sizer version 6.20 instrument.

5.2.4.6. Nitrogen sorption analysis:

The *Brunauer–Emmett–Teller* (BET) surface area, Barrett-Joyner-Halenda (BJH) surface area, BJH pore size and pore volume information was gathered from the Nitrogen adsorption and desorption studies. The unique BET hysteresis loop following isotherm IV was recorded under -196 ºC using Micromeritics ASAP 2020 instrument. Herein, MCM-41, MCM-NH_2-41, MCM-CHITO-41, MCM-FC-41 and MCM-48, MCM-NH_2-48, MCM-CHITO-48, MCM-FC-48 nanoparticles were given degassing treatment for 5 h at 200 °C temperature under vacuum. Whereas, the similar treatment was given to RLX incorporated bare and functionalized nanoparticles at 70 °C in order to prevent degradation of RLX at higher temperature.

5.2.4.7. SEM and TEM analysis:

The uniform spherical structure of the bare and surface coated MCM-41 and MCM-48 nanoparticles was determined by performing microscopical investigation on using scanning electron microscope (SEM) operated at 15 kV acceleration voltage. Further, 2D hexagonal and 3D cubic structure for bare and surface decorated MCM-41 and MCM-48 respectively was determined by transmission electron microscopic analysis on TEM CM 200 (Philips, India) model operated at 200 kV acceleration voltage having a 2.4 Aº resolution capacity.

5.2.5. Elemental detection and Quantification of surface moiety:

5.2.5.1. Elemental detection:

An elemental detection for pristine and surface decorated nanoparticles was performed in order to investigate the presence surface elements for bare and surface functionalized nanoparticles adopting SEM-EDX (scanning electron microscopy-energy-dispersive X-ray spectroscopy) analysis conducted on FEI-quanta 200 model (Thermo Scientific, USA). Further, the presence of carbon and nitrogen moiety after amine, chitosan, chitosan-folate and hyaluronic acid grafting was done by SEM-EDX analysis of respective nanoparticles.

5.2.5.2. Quantification of surface grafted moieties:

5.2.5.2.1. Quantification of amine group:

An estimation of the amine group grafted over the external surface was carried out by performing Ninhydrin colorimetric assay (16, 17) and thermal method (18, 19). The principle behind the Ninhydrin colorimetric assay is formation of colour product following the reaction between amine residue present over the surface and Ninhydrin reagent which was detected at 590 nm. The calibration curve was generated taking APTES as a standard in the concentration range of 0.1 to 0.5 µM (6). Here, an appropriate amount of APTES was transferred in the sodium acetate/acetic acid buffer solution followed by 2% ninhydrin reagent addition. This reaction assembly was heated at 78 ºC for 10min and cooled to room temperature. This was diluted appropriately to have a desired concentration with MeOH. Finally, the solution was centrifuged and the supernatant (V) was removed and analysed by UV-VIS spectrophotometer. Identical procedure was followed for quantification of amine group attached over the surface of bare MSN by taking a W gram of amine functionalized MSNs *i.e.* MCM-NH_2-41 and MCM-NH_2-48. The outcome was reported in terms of the amount of amine grafted in terms of mol/g (A_m), molecule/nm^2 (A_n) and %weight of an amine group (%W_a) and were calculated using below formulas (20).

$$A_m\left(\frac{mol}{g}\right) = \frac{MV}{W} \ldots\ldots\ldots\ldots\ldots 5.3$$

$$A_n\ (molecule/nm^2) = \frac{A_m}{SA} \times 6.02 \times 10^5 \ldots\ldots\ldots\ldots\ldots 5.4$$

$$\%W_a = A_m \times M_{ap} \times 100 \ldots\ldots\ldots\ldots\ldots 5.5$$

Where, M= Corresponding concentration of amino group (g/mol)

V = Volume of supernatant obtained after centrifugation (L)

W = Initial amount of MSN-NH_2 taken (g)

SA = BET surface area (m^2/g)

M_{ap} = Molecular weight of aminopropyl group

Amine group present on the external surface was further quantified by thermal method using thermo gravimetric analysis (TGA). Wherein, pristine MSNs and amine functionalized MSNs were given thermal treatment up to 700 ºC keeping heating rate of 5 ºC/min^{-1}. %Weight loss for both bare and functionalized MSNs were calculated and ultimately the %attachment was calculated by following equation 5.6 (18):

$$\%W_{AMINE} = \%W_{MSN-NH_2-41} - \%W_{MSN-41} \ldots\ldots\ldots\ldots\ldots 5.6$$

5.2.5.2.2. Quantification of other groups:

The thermal method was adopted for quantification of chitosan, chitosan-folate and hyaluronic acid moiety present on the outer surface. Wherein, surface modified nanoparticles were given thermal treatment up to 700 ºC keeping heating rate of 5 ºC/min^{-1} and the %weight loss for both was calculated and ultimately the %attachment was calculated by following equations.

$$\%W_{CHITO} = \%W_{MSN-CHITO-41} - \%W_{MSN-41} \ldots\ldots\ldots\ldots\ldots 5.7$$

$$\%W_{CHITO-FOLATE} = \%W_{CHITO-FOLATE-41} - \%W_{MSN-41} \ldots\ldots\ldots\ldots\ldots 5.8$$

5.2.6. Tablet formation and evaluation:

As the commercial formulation of RLX is in tablet form, a tablet formulation is necessary the RLX is available in the tablet form. A tablet formulation was prepared for synthesised bare and amine coated RLX nanoparticles following a direct compression method. The RLX tablets were prepared combining different excipients in the quantity as listed in following table 5.1. Single punch tablet machine equipped with punches of 9 mm diameter with flat faces was utilized and RLX tablets were punched. Subsequently, the detailed evaluation of prepared tablet was done for varied parameters as mentioned in the Indian pharmacopoeia (IP). Furthermore, the compatibility study of drug with excipient was carried and it demonstrated lack of interaction amongst themselves.

Table 5.1. List of excipients used in tablet preparation

Sr. No.	Name of Excipients	Application	Amount
1	Sodium Starch Glycolate	Disintegrating Agent	2-5%
2	Talc	Glidant	0.5-1%
3	Poly Vinyl Pyrolidone	Binder	2-5%
4	Magnesium Stearate	Lubricant + Diluent	0.5-1%
5	Microcrystalline cellulose	Common disintegrating agent used in Direct Compression	Q.S.

5.2.7. In vitro release study:

5.2.7.1. *In vitro* dissolution study:

Drug dissolution or drug release is a critical step as it has a significant influence on the bioavailability of the interested drug candidates suffering from solubility issues especially those belong to a BCS class II and IV category (21). *In vitro* dissolution study was performed for oral formulations of RLX in different dissolution media as listed in table 5.2. The *in vitro* release study was carried using Veego USP type II dissolution apparatus wherein the plain API, marketed formulation, RLX-41, RLX-48, RLX-NH_2-41, RLX-NH_2-48 were subjected for rotation at a speed of 50 rpm in 900 mL dissolution media maintained at 37 ± 0.5 ℃ temperature. The study was also conducted in biorelevant media. The composition of all dissolution media is listed in the following table 5.2.

Table 5.2: Composition of different simulated and biorelevant dissolution media (22, 23)

Sr. No	Ingredients	A	B	C	D	E	F	G
1.	Conc. HCl	7 mL	-	-	q.s. to get pH 1.6	q.s. to get pH 1.6	-	-
2.	Sodium acetate trihydrate	-	2.99 gm	-	-	29.75 mM	-	-
3.	acetic acid	-	14.0 mL (2 N acetic acid)	-	-	17.12 mM	-	8.65 gm
4.	Sodium hydroxide	-	-	0.616 gm	-	-	34.8 mM	4.04 gm

5.	Monobasic potassium phosphate	-	-	6.8 gm	-	-	-	-
6.	Sodium chloride	2 gm	-	-	1.9986 gm (34.2 mM)	237.02 mM	68.62 mM	11.874 gm
7.	Pepsin	3.2 gm	-	-	0.1 gm (0.1 mg/mL)	-	-	-
8.	Pancreatin	-	-	1 gm		-	-	-
9.	Sodium taurocholate	-	-	-	0.4125 gm (0.08 mM)	-	3 mM	15 mM
10.	Lecithin	-	-	-	0.1287 gm (0.02 mM)	-	0.2 mM	3.75 mM
11.	milk	-	-	-	-	500 mL	-	-
12.	Maleic acid	-	-	-	-	-	19.12 mM	-
13.	Polysorbate 80	0.1%	0.1%	0.1%	-	-	-	-
14.	Deionised water	Upto 1000 mL	Upto 1000 mL	Upto 1000 mL	Upto 1000 mL	Upto 1000 mL	Upto 1000 mL	Upto 1000 mL

*A: Simulated gastric fluid (SGF pH: 1.8), B: Sodium acetate buffer (pH: 4.5), C: Simulated intestinal fluid (SIF) (pH: 6.8), D: Fasted state simulated gastric fluid (FaSSGF) (pH: 5), E: Fed state simulated gastric fluid (FeSSGF), F: Fasted state simulated intestinal fluid (FaSSIF-V2), G: Fed state simulated intestinal fluid (FeSSIF)

5.2.7.2. *In vitro* diffusion study:

The drug release study from the parenteral formulation was evaluated following *in vitro* diffusion study performed in dialysis bag. Thus, the chitosan and chitosan-folate modified nanoparticles for RLX. The release study was performed at three different pH of the phosphate buffer saline (PBS) solution *i.e.* at pH 5.6, 6.8 and 7.4. Herein, 10 mg of the formulation was dispersed in 5 mL dispersion media and filled in the dialysis bag. The bag was immersed in 100 mL diffusion media and rotated at 75 rpm. The temperature of the assembly was maintained at 37 ºC and the aliquots were withdrawn at different time interval up to 72 h. The

samples were analyzed by RP-HPLC method and %CDR was calculated.

5.2.8. In vitro cytotoxicity Study:

Two different cell lines were used to perform *in vitro* cytotoxicity study viz., (i) Caco-2 cell line (for oral formulation) and (ii) MCF-7 cell line (for parenteral formulation).

5.2.8.1. Caco-2 cell line:

Herein, MTT assay was performed on Caco-2 cells before initiating the cell permeability study in order to select the maximum safe concentration of RLX encapsulated pristine and amine coated nanoparticles which will not harm the cell viability. The formulation having RLX concentration ranging from 10 ppm to 100 ppm were taken to proceed further with the MTT assay. Here, the experiment started with the seeding step, where the Caco-2 cells were cultured in 96 well plates using DMEM medium enriched with sodium pyruvate, L-glutamate, sodium bicarbonate along with high glucose and supplemented with 20% fetal bovine serum (FBS) and 1% penicillin-streptomycin (Pen/strep) solution which resist bacterial growth. Once the cell growth reached to $1*10^4$ cell/well density, the cell was given nanoparticle treatment. Eventually, the cells were treated with MTT dye after a desired period of time (4 h) and evaluated for cell viability parameter at 570 nm using plate reader. Furthermore, the blank and negative control readings were also taken in order to avoid false negative errors. The cells without nanoparticle treatment were taken as a negative control and DMSO was taken as blank. The cell viability was calculated by below equation 5.9.

$$\%Cell\ Viability = \frac{O.D._{.sample} - O.D._{.blank}}{O.D._{.negative\ control} - O.D._{.blank}} \times 100 \ldots\ldots\ldots\ldots\ldots 5.9$$

5.2.8.2. MCF-7 cell line:

The cell viability study was carried out on human breast carcinoma cell line *i.e.* MCF-7 for drug free and drug loaded nanoparticles. The MTT assay was initiated with the seeding step. The MCF-7 cells were seeded in the 96 well plate supplemented with DMEM containing sodium pyruvate, L-glutamate, sodium bicarbonate along with high glucose supplemented with 10% foetal bovine serum (FBS) and 1% penicillin-streptomycin (Pen/strep) solution which resists bacterial growth. For this, 100µL cell suspension (10000 cells/well) was added to each well and incubated for 24 h at 37 ºC. Second step of the MTT assay was drug treatment. Here, RLX loaded nanoparticles containing 1-8µM equivalent RLX and drug free nanoparticles in the range of 0.1-100 µM were added and eventually well plate was incubated for a desired

period time (24h and 72h). After the completion of desired time period, the MTT dye treatment was given and the well plate was read at 570nm. Here, the cells without nanoparticle treatment were taken as a negative control and DMSO was taken as blank. Eventually, the %cell viability was calculated using the following equation.

$$\%Cell\ Viability = \frac{O.D._{.sample} - O.D._{.blank}}{O.D._{.negative\ control} - O.D._{.blank}} \times 100 \ldots\ldots\ldots\ldots\ldots 5.10$$

5.2.9. Cell permeability across Caco-2 cell monolayer:

It is an important task to determine the cell permeability of formulated nanoparticles, the Caco-2 cells were grown on the Trans well® inserts (Nunc, Denmark) having 0.4µ pore diameter with 1.13 cm^2 area. The inserts were thoroughly washed with the transport solution *i.e.* Hank's balanced salt solution (HBSS) containing 25mM of HEPES, pH 7.4. The integrity of the Caco-2 cell monolayer was tested by monitoring the Lucifer yellow dye permeability across the cell layer. Time dependent transport of RLX loaded nanoparticles was performed in unidirectional manner *i.e.* apical-to-basal. For this study, the donor compartment *i.e.* the apical side is treated with 0.5 mL of transport solution *i.e.* 1.5 M HBSS containing 0.1 mg/mL RLX and basal side was treated with 1.5 mL of HBSS solution. After incubation of 30, 60, 90, 120, 180, and 240 min, 100µL aliquots were withdrawn from the receiver and replenished with the equal volume of fresh HBSS. The samples were analysed by HPLC. The apparent permeability coefficient (P_{app}) was measured using the following equation.

$$P_{app} = \frac{dQ/dt}{A \times C_0} * 60 \ldots\ldots\ldots\ldots\ldots 5.11$$

Where, P_{app}: Apparent permeability coefficient (cm/h)

dQ/dt: drug permeation rate (µg/s)

A: cross-sectional area *i.e.* 1.13 cm^2

C_0: Initial RLX concentration in the donor compartment (µg/mL)

5.2.10. In vitro cellular uptake study:

5.2.10.1. Synthesis of FITC labelled nanoparticles:

The surface silanol group of bare nanoparticles was replaced with the amine group using APTES. Now, this amine group would be available for the attachment of FITC molecule. The nanoparticle were labelled as per the procedures adopted earlier with slight modifications (24, 25) For this, a methanolic solution of FITC (0.3 mg/mL) was used. In which, the 10 mg aminated MSNs and HA-MSNs were added and exposed to continuous stirring in the dark for

12h. Furthermore, the solution was centrifuged and washed with methanol for complete removal of unconjugated FITC until the supernatants obtained were rendered colourless.

5.2.10.2. Intra cellular uptake study by confocal analysis:

Qualitative uptake of nanoparticles by MCF-7 cells was studied by confocal analysis. The MCF-7 cells were seeded in the 6 well plates containing coverslips ($5x10^5$ cells/well) one day before the drug treatment. Afterwards the cells were treated with the fixed concentration (10 µM) of FITC labelled MCM-NH_2-41, MCM-CHITO-41, MCM-FC-41, FA+ MCM-FC-41 and MCM-NH_2-48, MCM-CHITO-48, MCM-FC-48, FA+MCM-FC-48 nanoparticles for 24h. After completion of the predefined time, the coverslips were washed thoroughly with the PBS and fixed with 3% paraformaldehyde for 5 min at room temperature and stained with DAPI followed by microscopical analysis on a Leica confocal microscope (26).

5.2.10.3. Intracellular uptake study by flow cytometry:

Flow cytometric analysis is an ideal approach for the quantification of internalization of nanoparticles. The experiment was initiated following seeding step. Here, cells ($5x10^5$ cells/well) were seeded in 12-well plate and incubated at 37 ºC for 24 h. Once the sufficient confluency is reached, the wells were treated with 10 µM of FITC labelled MCM-NH_2-41, MCM-CHITO-41, MCM-FC-41, FA+MCM-FC-41 and MCM-NH_2-48, MCM-CHITO-48, MCM-FC-48, FA+ MCM-FC-48 nanoparticles and incubated at 37 ºC for 24 h. Afterwards, the cells were detached by trypsinization step. The cells were centrifuged at 1000 rpm for 3-5 min and the cell pellet was resuspended in FACS buffer by aspirating through pipetting and vortexing it to carry out the uptake study on FACS Calibur flow cytometer. All the experiments were carried out in triplicate. Here the untreated cells were taken as control.

(FACS buffer preparation: 0.5 gm bovine serum albumin and 0.5 mL FBS were mixed together and volume was made to 100 mL by PBS solution)

5.2.11. Apoptosis assay

Annexin V-FITC double stain apoptosis detection kit from BD Biosciences was used for study. The MCF-7 cells were seeded each at a density of $5x10^5$ cells/well and incubated for 24 h. Then the cells were given PBS wash twice and subsequently, treated with 5 µM of RLX, RLX-CHITO-41, RLX-FC-41 and RLX-CHITO-48, RLX-FC-48. This was followed by cold PBS (4℃) wash after 24 h and stained with FITC-Annexin V. Concisely, the cells were suspended in 1 mL of 1 × binding buffer at a concentration of 1×10^5 cells/mL. Further, 5µL of FITC-

Annexin V and 5µL of PI were added per 100µL of the suspension (1×10^5). After mild vortexing, the cells were incubated for 15 min in the dark. Finally, 400 µL of 1 × binding buffer was added to each tube and analysed by flow cytometry.

5.2.12 Hemolysis study:

It is very essential to study the compatibility of formulated nanoparticles with the erythrocytes (27). Hence, the hemolysis study was performed as per the literature method for engineered parenteral formulations. (10, 28, 29). The freshly collected blood sample was centrifuged at 8000 rpm for 5 min at 4 ºC. The plasma supernatant was removed and the residue was washed with PBS buffer (pH: 7.4) and diluted 10 folds. To the 200 µL RBC solution, 800 µL of nanoparticle solution (RLX, RLX-CHITO-41, RLX-FC-41, RLX-CHITO-48, and RLX-FC-48) having the concentrations of 0.1-100 µg/mL were prepared individually. The few drops of the sample were plated on the glass slide and analyzed by the microscope. Additionally, for the quantitative analysis, all the samples were incubated for 2 h at 37 ºC and centrifuged at 10000 rpm for 2 min at 4 ºC and the collected supernatant was analyzed by UV-Vis spectrophotometer at 570 nm. Eventually, the %hemolytic activity was calculated considering following formula. 2%v/v Triton X_{100} was taken as a positive control and PBS buffer (pH: 7.4) was taken as a negative control respectively.

$$\%Hemolysis = \frac{A_{sample} - A_{Negative\ Control}}{A_{Positive\ Contol} - A_{negative\ Contol}} \times 100 \ldots\ldots\ldots\ldots\ldots 5.12$$

5.2.13. In vivo pharmacokinetic study:

5.2.13.1. Pharmacokinetic study for oral formulation:

5.2.13.1.1. Experimental:

Female Swiss albino mice were housed in a ventilated cage and given free access to food and water and acclimatized for a week before performing the actual experiment. The animals were divided into 7 groups and each group containing 3 animals and they were fasted overnight and given free access to water for 12 hours before giving the first dose. Group-I animals were labelled as controlled group and they were given 0.9% w/v saline solution (negative control). Group-II animals were given RLX suspension prepared in saline solution having dose equivalent to 7.4mg/kg were administered. Similarly, group-III, group-IV, group-V, group-VI and group-VII was given marketed formulation, RLX-41, RLX-48, RLX-NH_2-41, and RLX-NH_2-48 (each equivalent to 7.4mg/kg RLX) respectively. All the formulations were

administered using syringes and infant feeding tube. The blood samples were withdrawn using a capillary tube at 0.5, 1, 2, 4, 8 and 12h post dosing from the retro-orbital venous plexus and collected in the EDTA treated tubes.

5.2.13.1.2. Sample preparation:

The protein precipitation method was optimized to recover the sample from the bioanalytical matrix. Briefly, the collected blood samples were centrifuged at 5000 rpm for 10 min at 4 ºC temperature and plasma was collected. To the 100µL of the plasma sample, 50 µL of internal standard (Edaravone: 10 ppm) was incorporated and vortexed for 1 min. furthermore, 300 µL of ACN was added and vortexed for 3 min. Thereafter, the reaction assembly was centrifuged at the 5000 rpm for 10 min keeping 4 ºC temperature. 10 µL of the supernatant was removed and analysed by HPLC.

5.2.13.1.3. Pharmacokinetic parameters evaluation:

Different pharmacokinetic parameters were calculated from the plasma concentration time data by means of a model independent method *i.e.* non-compartmental model using PK solver software®. Peak plasma concentration (C_{max}), $T_{1/2}$ and time required for achieve C_{max} *i.e.* t_{max} were obtained by visual inspection of the experimental data. Moreover, the linear trapezoidal method was applied to determine area under curve (AUC_{0-t}).

5.2.13.2. Pharmacokinetic study for parenteral formulation:

For pharmacokinetic study of the parenteral formulation, a total of 12 mice were randomly divided into 3 groups (n=4) and intravenously injected saline, RLX, RLX-FC-41 and RLX-FC-48 from the tail vein with a 0.5 CC U40 insulin syringe fitted with a 28-$g^{1/2}$. The blood sample (0.3 ml) was collected at specific time intervals and stored in EDTA added centrifuge vials. Further, plasma was separated by centrifugation at 4000 rpm for 10 minutes at 4℃. 100µL plasma was mixed with internal standard EDA. The samples were precipitated by adding Acetonitrile (ACN) and again centrifuged at 5000 rpm for 10 min. The supernatants were collected and RLX was quantified using a HPLC. Different pharmacokinetics parameters viz C_{max}, T_{max} and AUC were calculated by using PK Solver excel add-in.

5.2.14. In vivo biodistribution study and histological examination

The biodistribution of formulated final nanoparticles in major organs was studied following parenteral administration of RLX, RLX-FC-41 and RLX-FC-48 in the mice. Sterile saline injections at equivalent volumes were given to mice as control. Mice were sacrificed at 24 h

after injection and major organs like heart, liver, lung, kidney, prostate, brain and spleen were collected and weighed. Furthermore, PBS solution was added to each tissue sample by an equal volume to its weight and subjected to high speed homogenization. The mixtures obtained were centrifuged at 10000 rpm for 10 min. The supernatant was collected and extracted with ACN. The extracted sample was analyzed and quantified by HPLC to report the concentration of RLX in different organs. The aforementioned major organs collected were fixed in 10% formalin in PBS solution. The organs were embedded in paraffin and sectioned to 4µm sections and placed onto the glass slides. The histological sections were stained with H&E and observed under microscope.

5.2.15. Statistical analysis

The experiments were conducted thrice, and the results were expressed as the means and standard deviations from the triplicate experiments unless mentioned otherwise. The statistical analysis was performed by one-way ANOVA and p-values less than 0.05 were considered as significant.

5.2.16. Stability study of prepared nanoparticles:

The stability study of synthesized nanoparticles i.e. RLX-41, RLX-NH_2-41, RLX-CHITO-41, RLX-FC-41 and RLX-48, RLX-NH_2-48, RLX-CHITO-48, RLX-FC-48 were performed as specified in ICH Q1A(R2). The synthesized nanoparticles were exposed to 40±2 ºC and 75±5 %RH conditions and sampling was done at 0^{th} day, 3^{rd} month and 6^{th} month and samples were analyzed by DSC and SXRD.

5.3. Result and discussion:

5.3.1. Solid state evaluation of MSNs:

5.3.1.1. FTIR:

Characterization of formulated nanoparticles was initiated with the preliminary FTIR investigation. FTIR is an essential qualitative technique for affirming the MSNs synthesis, RLX uptake by MSNs and amine grafting on the surface of MSNs as well. Figure 5.1 represents a characteristic FTIR vibrational peak due to mesoporous assembly for MCM-41 and surface decorated MCM-41 type of nanoparticles. Figure 5.1A demonstrated a prominent IR peaks at 2922 and 2852 cm^{-1} due to C-H stretching vibration and C-H deformation vibration peak at 1454 cm^{-1} could be accredited to template moiety occupied in the mesopores of CTAB@MCM-41. The success of the formation of MCM-41 is confirmed by the presence of the fingerprint IR vibration peaks at 1100 and 780 cm^{-1} wavenumber due to symmetric and asymmetric stretching of Si-O-Si respectively in figure 5.1B. Additional blunt and diffused stretching vibrational peak over the region of 3300-3500 cm^{-1} indicates the presence of terminal Si-OH (silanol) group. Furthermore, disappearance of representative C-H stretching peak also supports the hypothesis of removal of surfactant after calcination (figure 5.1B). The favourable output of amine grafting on the external surface was gathered from the N-H bending peak and the C-H stretching peak at 1585 cm^{-1} and 2915 cm^{-1} respectively for MCM-NH_2-41 as portrayed in figure 5.1C. On the other hand the O-H and N-H stretching, C-H stretching, and N-H bending peak in the region of 3379, 2907, and 1576 cm^{-1} in figure 5.1D is assigned to chitosan grafting on MCM-CHITO-41. The prominent vibrational peaks of folate-chitosan conjugates are shown in figure 5.1E. The prominent O-H vibrational peak was retained in the region of 3300 to 3450 cm^{-1} along with the peaks at 1100 and 780 cm^{-1} wavenumber due to symmetric and asymmetric stretching of Si-O-Si respectively affirmed successful functionalization of chitosan-folate on the outer surface of MCM-FC-41 (figure 5.1F).

Figure 5.2 demonstrates FTIR spectra of RLX loaded MCM-41 type of nanoparticles. Figure 5.2A displays a FTIR spectra of RLX wherein the characteristic stretching vibration IR peaks at 3490, 2930, 1605 and 1268 cm^{-1} corresponds to a phenolic –OH group, C-H group, C=O and C-O group respectively. Nonexistence of RLX symbolic peaks for RLX-41, RLX-NH_2-41, RLX-CHITO-41 and RLX-FC-41 emphasizes RLX uptake by MCM-41 (figure 5.2B), MCM-NH_2-41 (figure 5.2C), MCM-CHITO-41(figure 5.2D), and MCM-FC-41 (figure 5.2E), respectively.

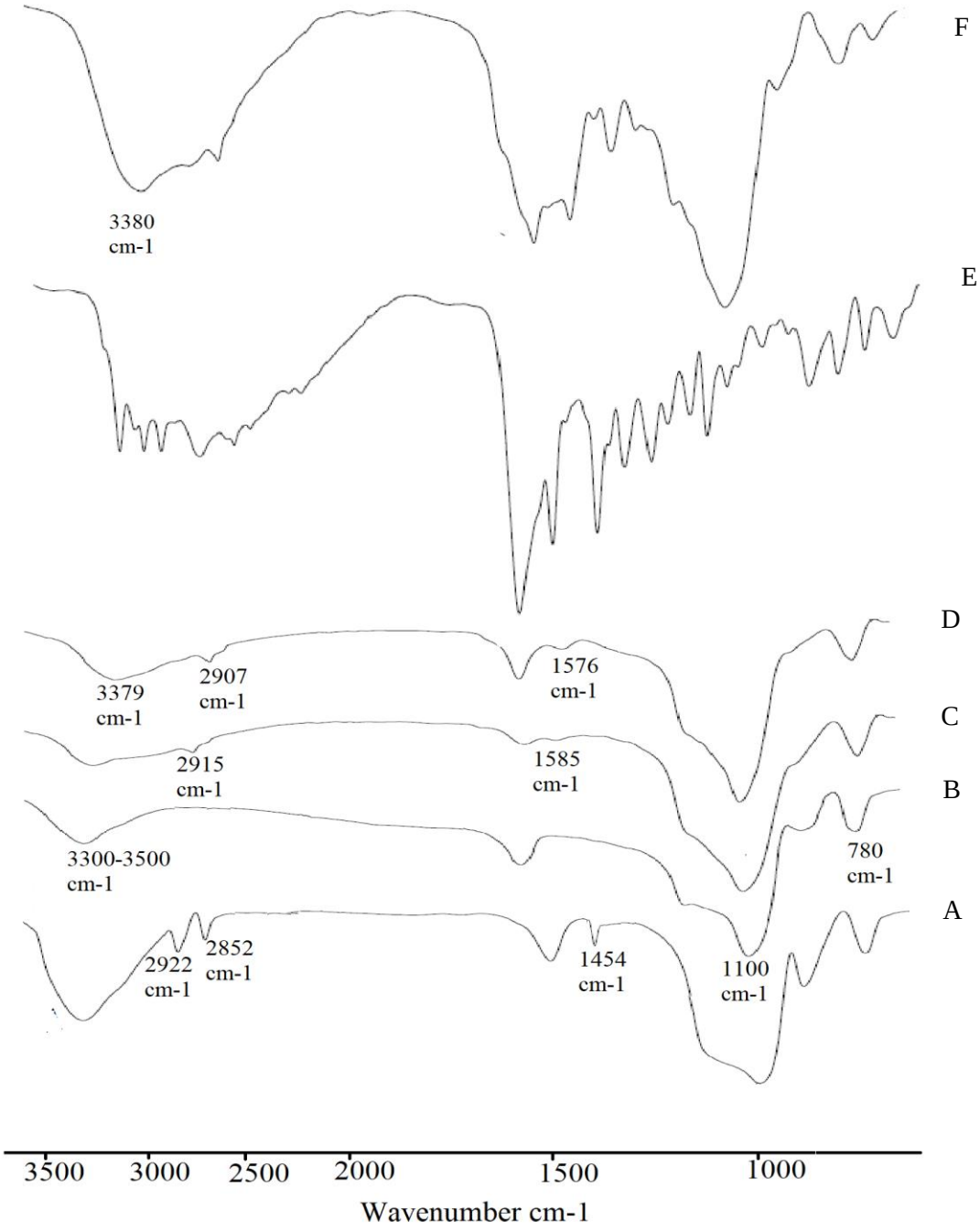

Figure 5.1 FTIR spectra of (A) CTAB@MCM-41, (B) MCM-41, (C) MCM-NH_2-41, (D) MCM-CHITO-41, (E) Folate-chitosan conjugate, (F) MCM-FC-41

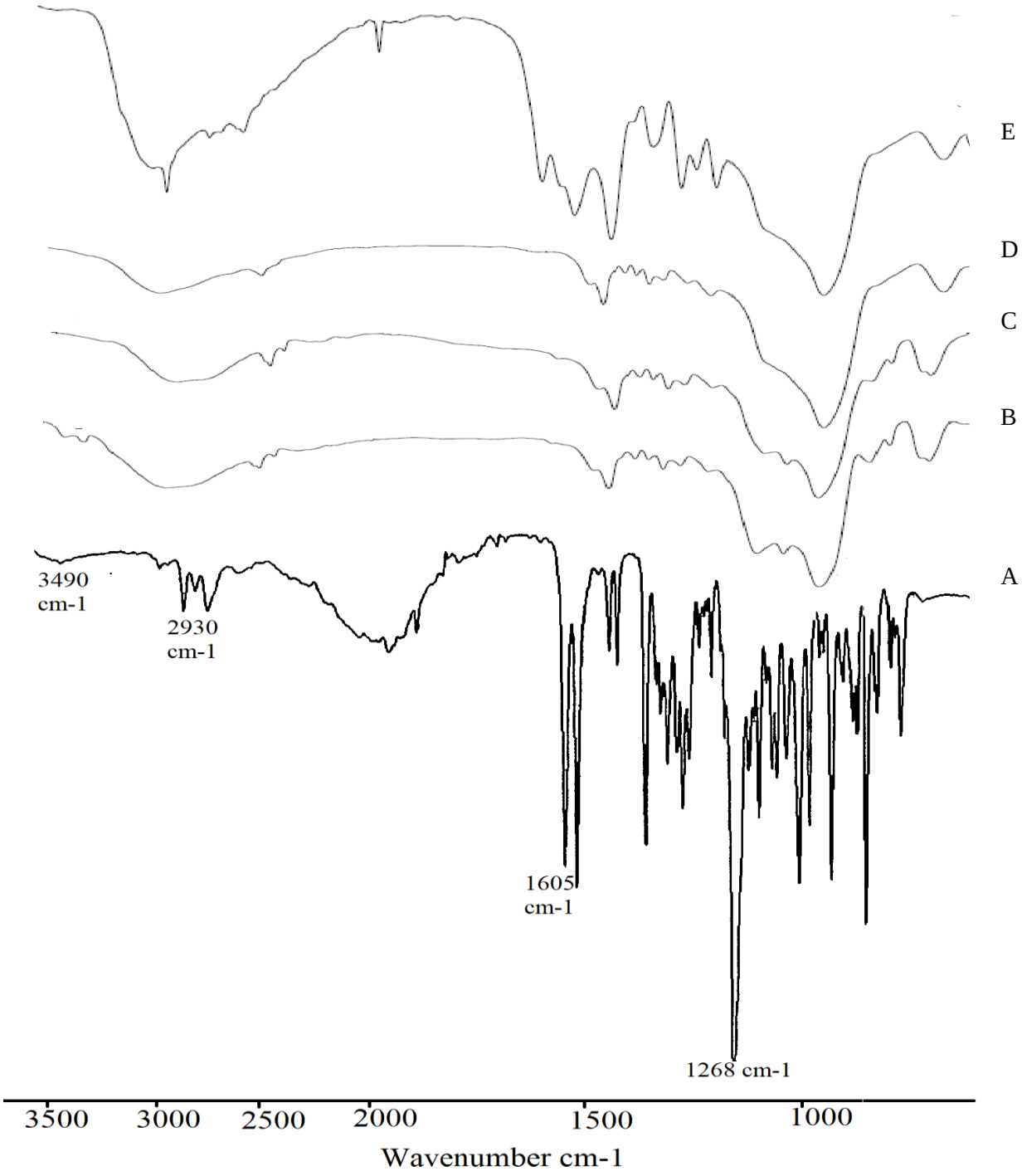

Figure 5.2 FTIR spectra of (A) RLX, (B) RLX-41, (C) RLX-NH_2-41, (D) RLX-CHITO-41, (E) RLX-FC-41

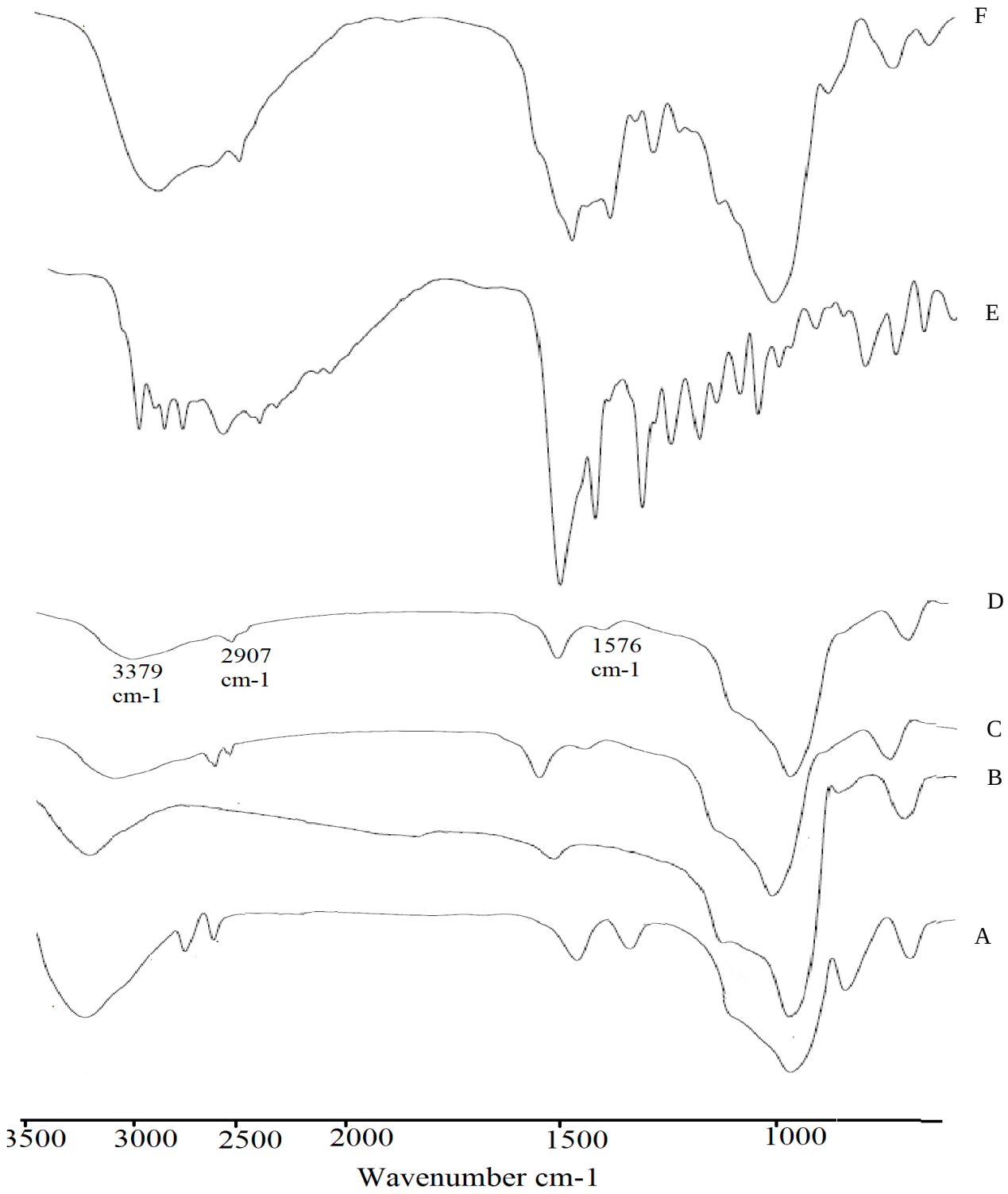

Figure 5.3 FTIR spectra of (A) CTAB@MCM-48, (B) MCM-48, (C) MCM-NH_2-48, (D) MCM-CHITO-48, (E) Folate-chitosan conjugate, (F) MCM-FC-48

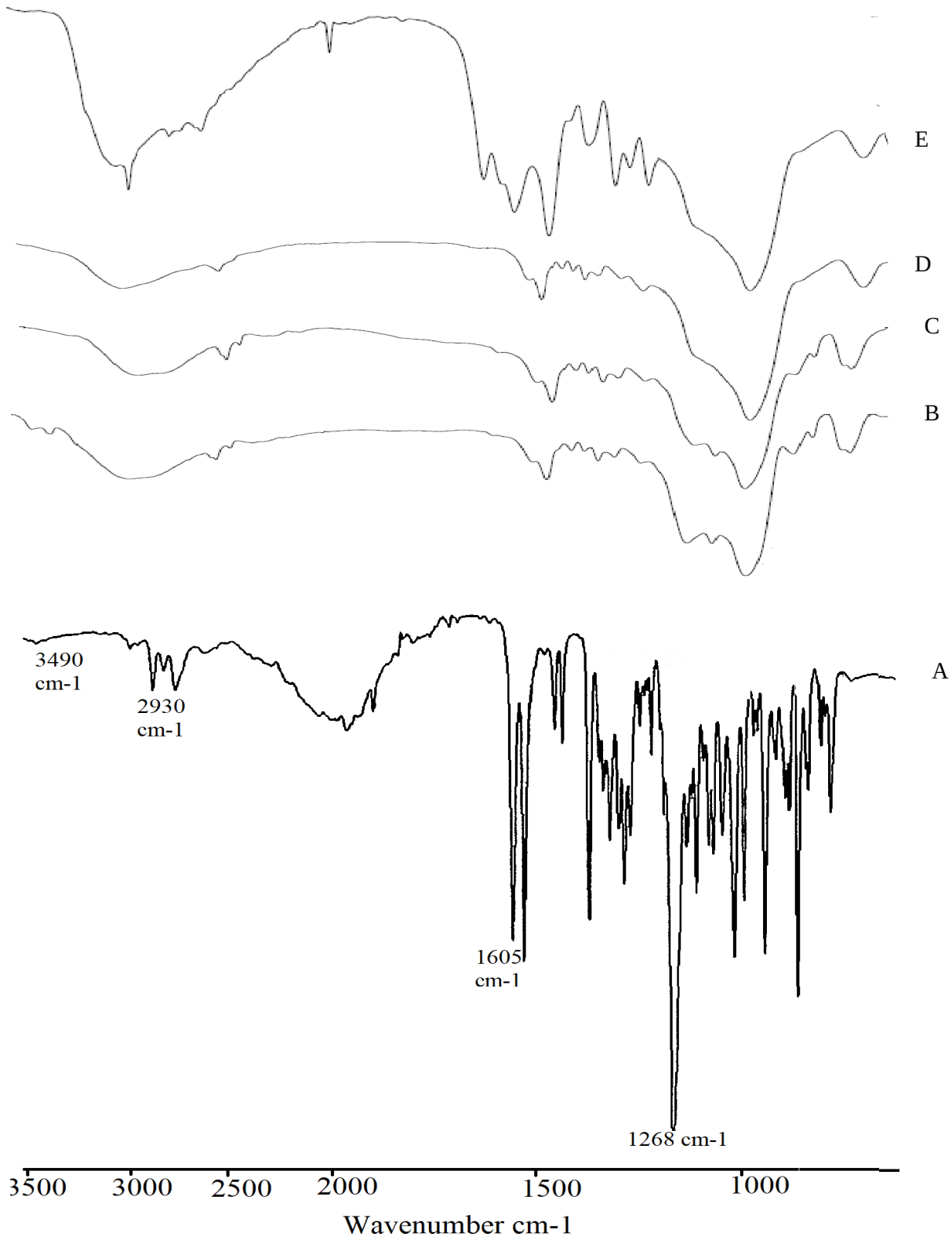

Figure 5.4. FTIR spectra of (A) RLX, (B) RLX-48, (C) RLX-NH_2-48, (D) RLX-CHITO-48, (E) RLX-FC-48

Similar outcomes for pristine and surface coated MCM-48 type nanoparticles revealed successful grafting of organic moieties along with the formation of mesoporous assembly (figure 5.3). Additionally, the FTIR spectra of RLX loaded nanoparticle demonstrated complete encapsulation of RLX inside the MCM-48 types of nanoparticle (figure 5.4).

5.3.1.2. DSC:

Further confirmation ensuring the absolute RLX uptake was done by DSC examination of plain RLX and RLX filled nanoparticles. Theory says that drug loaded silica NPs would exhibit a smooth DSC thermogram over the working range of temperature due to the conversion of the crystalline form to non-crystalline form (30). Figure 5.5A illustrated a keen endothermic peak at 262.06 ºC temperature which is assigned to the melting of crystalline RLX. Lack of such sharp peak for RLX-41, RLX-NH_2-41, RLX-CHITO-41 and RLX-FC-41 in figure 5.5B-E displayed engulfment of RLX within the pores. Similar outcomes were encountered for bare and surface coated MCM-48 type of nanoparticles as portrayed in figure 5.6A-E. Thus, the RLX was successfully encapsulate within the MCM-48 types of mesoporous carrier also.

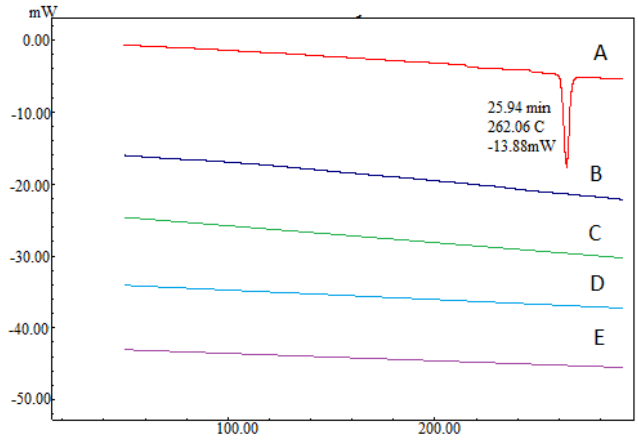

Figure 5.5: DSC thermogram of (A) RLX, (B) RLX-41, (C) RLX-NH_2-41, (D) RLX-CHITO-41, (E) RLX-FC-41

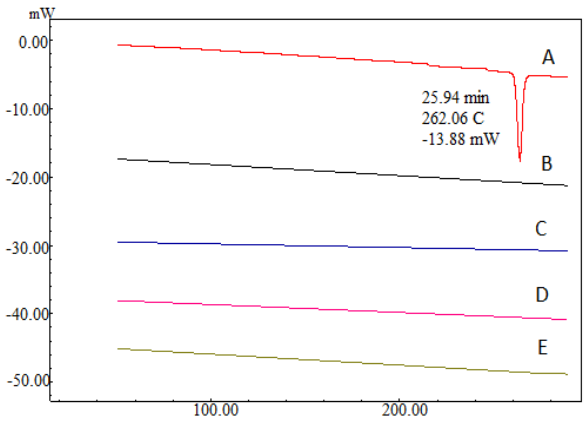

Figure 5.6: DSC thermogram of (A) RLX, (B) RLX-48, (C) RLX-NH_2-48, (D) RLX-CHITO-48, (E) RLX-FC-48

5.3.1.3. WXRD:

Similar conclusion regarding drug uptake was established through WXRD study. The WXRD spectra ranging from 10º to 40º 2θ/º region is represented in below figures. Where, figure 5.7A revealed few indicative peaks for pure RLX which were lacking in the RLX incorporated

MCM-41 and MCM-48 type nanoparticles as shown in figure 5.8B-E and figure 5.8B-E respectively.

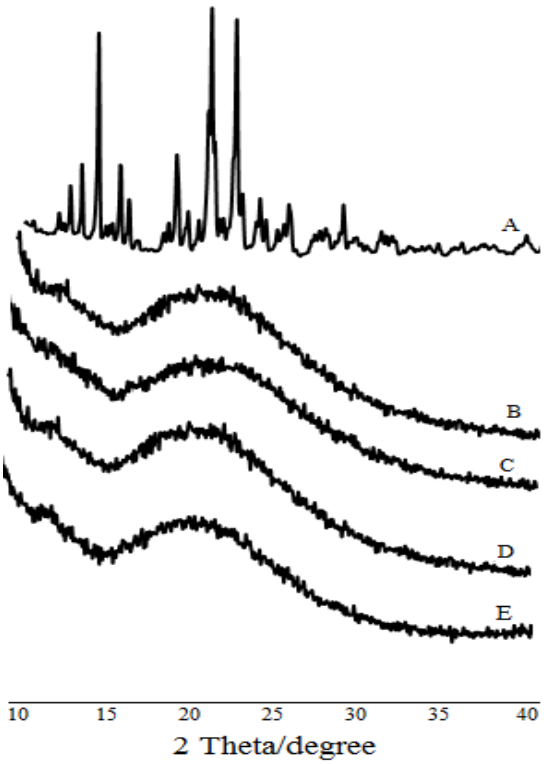

Figure 5.7: WXRD spectra of (A) RLX, (B) RLX-41, (C) RLX-NH$_2$-41, (D) RLX-CHITO-41, (E) RLX-FC-41

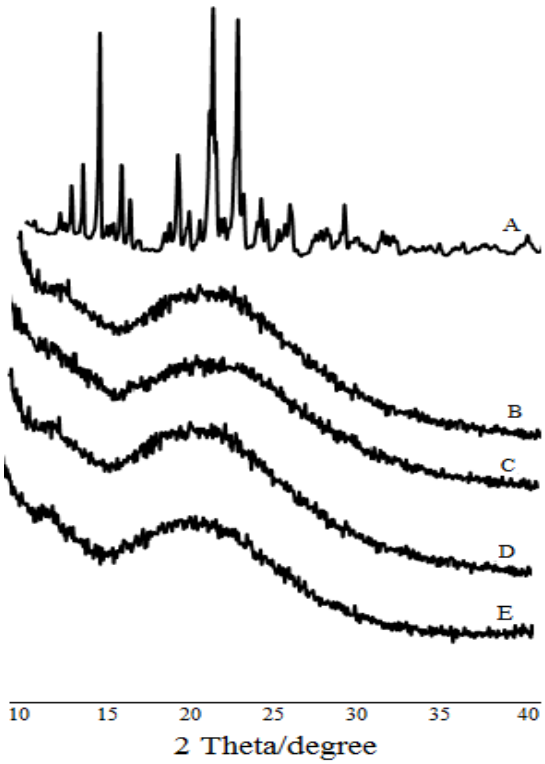

Figure 5.8: WXRD spectra of (A) RLX, (B) RLX-48, (C) RLX-NH$_2$-48, (D) RLX-CHITO-48, (E) RLX-FC-48

5.3.1.4. SXRD:

The surface functionalization and RLX impregnation by bare and surface coated NPs were confirmed by SXRD. Apart from giving aforementioned information, SXRD also utilized as an evidence to demonstrate the persistence of mesoporous integrity after surface capping and RLX uptake as well. The mesoporous skeleton for MCM-41 and MCM-48 were affirmed by the typical SXRD peaks in the region of 1º to 10º 2θ/º. Concisely three distinct peaks were identified at 100, 110 and 200 2θ/º attributed to the mesoporous assembly of MCM-41 as illustrated in figure 5.9A. Moreover, the peak at 100 2 theta/degree obtained for MCM-NH$_2$-41, MCM-CHITO-41 and MCM-FC-41 exhibits a noteworthy reduction in the intensity which strongly suggests amine grafting (figure 5.9B-D). Furthermore, a surface coating might be responsible for the drastic reduction in the intensity of the peaks which ultimately responsible for the disappearance of two successive peaks at 110 and 200 for surface coated nanoparticles. Similar results were encountered for RLX-41, RLX-NH$_2$-41, RLX-CHITO-41 and RLX-FC-

41 (figure 5.10A-D) with a reduction in the intensity compared to drug free nanoparticles which could be due to RLX encapsulation inside the pores.

On the other hand, figure 5.11A exemplified two peaks at 211, 220 and other two peaks at the higher side for MCM-48. These aforementioned peaks existed for MCM-NH_2-48, MCM-CHITO-48 and MCM-FC-48 with reduced intensity which again emphasizes the formation of functionalized nanoframework (figure 5.11B-D). Additionally, the reduction in the intensity of drug loaded nanoparticles with respect to RLX free nanoparticles ascertained complete RLX loading within the mesopores without distortion of the mesoporous skeleton (figure 5.12A-D).

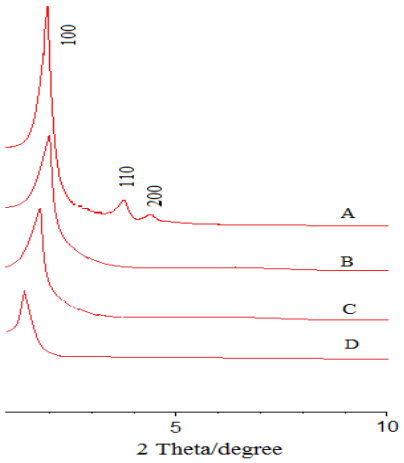

Figure 5.9: SXRD spectra of (A) MCM-41, (B) MCM-NH_2-41, (C) MCM-CHITO-41 and (D) MCM-FC-41

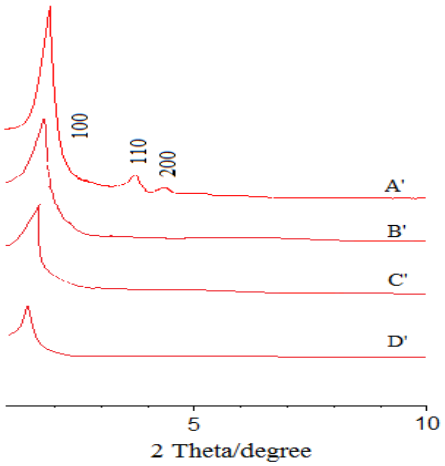

Figure 5.10: SXRD spectra of (A) RLX-41, (B) RLX-NH_2-41, (C) RLX-CHITO-41 and (D) RLX-FC-41

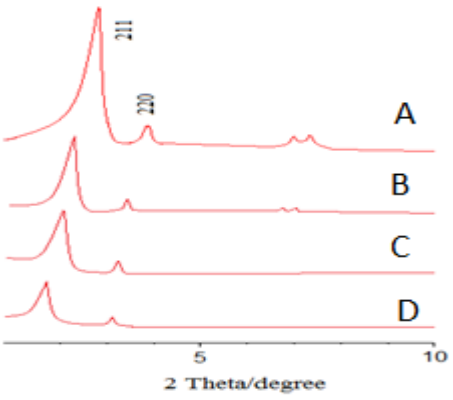

Figure 5.11: SXRD spectra of (A) MCM-48, (B) MCM-NH_2-48, (C) MCM-CHITO-48 and (D) MCM-FC-48

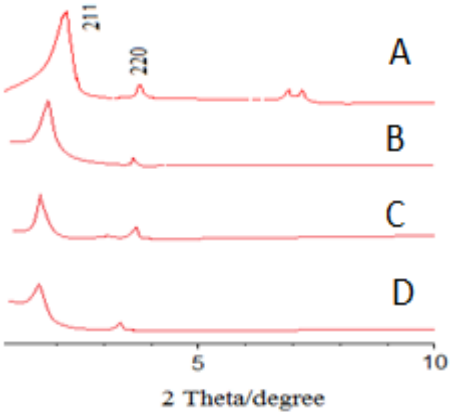

Figure 5.12: SXRD spectra of (A) RLX-48, (B) RLX-NH_2-48, (C) RLX-CHITO-48 and (D) RLX-FC-48

5.3.1.5. Nitrogen sorption study:

The type IV isotherm with the hysteresis loop for formulated nano assembly were acquired through comprehensive BET analysis. BET investigation demonstrated higher surface area with the optimized pore size which might have greater influence in the dissolution and in turn bioavailability enhancement. The surface area recorded for MCM-41 nanoparticles (713.97 m^2/g) declined progressively after amine coating (529.18 m^2/g), chitosan coating (258.14 m^2/g) and folate-chitosan coating (185.16 m^2/g) as depicted in figure 5.13A-D. Identical outcomes were obtained for RLX loaded bare and amine coated nanoparticles. Where, the surface area was steadily decreased for RLX-41 (394.74 m^2/g) to RLX-FC-41 (130.59 m^2/g) compared to drug free bare and surface decorated MCM-41 (figure 5.14A-D). Similar behaviour was also observed for MCM-48 nanoparticles where the surface area of bare nanoparticle was decreased from 997.71 m^2/g to 212.45 m^2/g for final formulation (figure 5.15A-D and 5.16A-D).

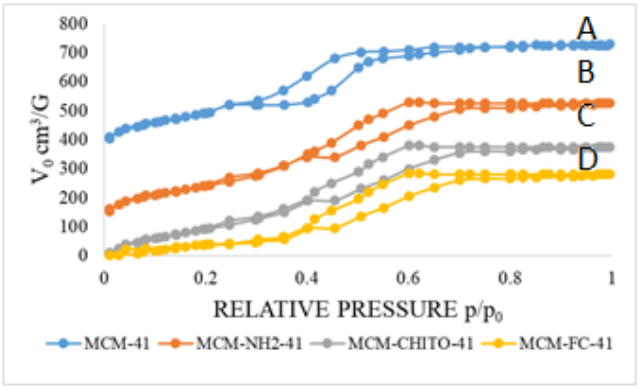

Figure 5.13 BET graph of (A) MCM-41, (B) MCM-NH$_2$-41, (C) MCM-CHITO-41 and (D) MCM-FC-41

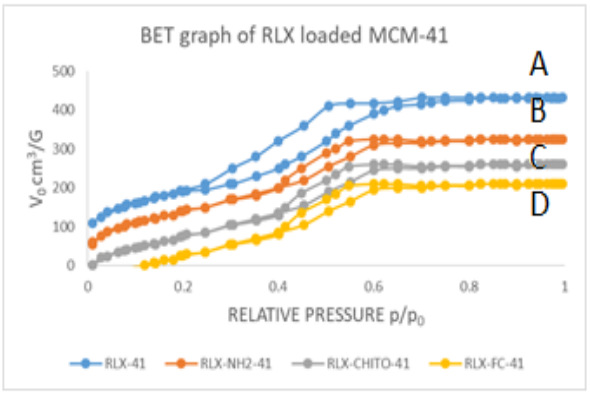

Figure 5.14: BET graph of (A) RLX-41, (B) RLX-NH$_2$-41, (C) RLX-CHITO-41 and (D) RLX-FC-41

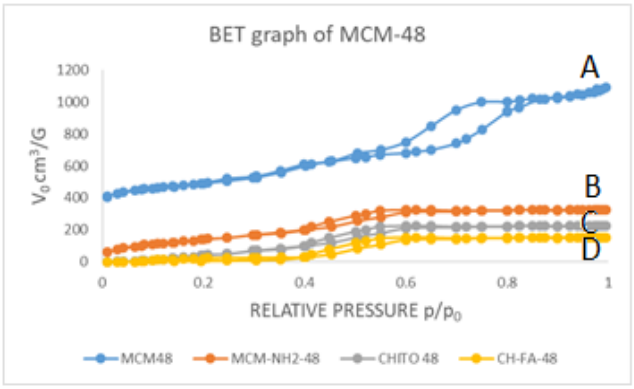

Figure 5.15: BET graph of (A) MCM-48, (B) MCM-NH$_2$-48, (C) MCM-CHITO-48 and (D) MCM-FC-48

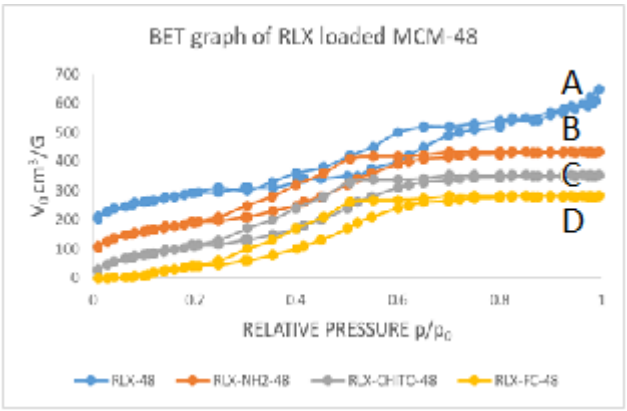

Figure 5.16: BET graph of (A) RLX-48, (B) RLX-NH$_2$-48, (C) RLX-CHITO-48 and (D) RLX-FC-48

Besides these, pore size distribution and pore volume data were also gathered for all varied kinds of nanoparticles as summarized in table 5.3 and also depicted in figure 5.17 for RLX loaded and unloaded MCM-41. The similar information was given in figure 5.18 and table 5.4 for MCM-48. Wherein, a sharp rise in the pore volume at a single point for each nanoparticles due to capillary condensation of nitrogen unveiled uniform pore size distribution of formulated mesoporous system

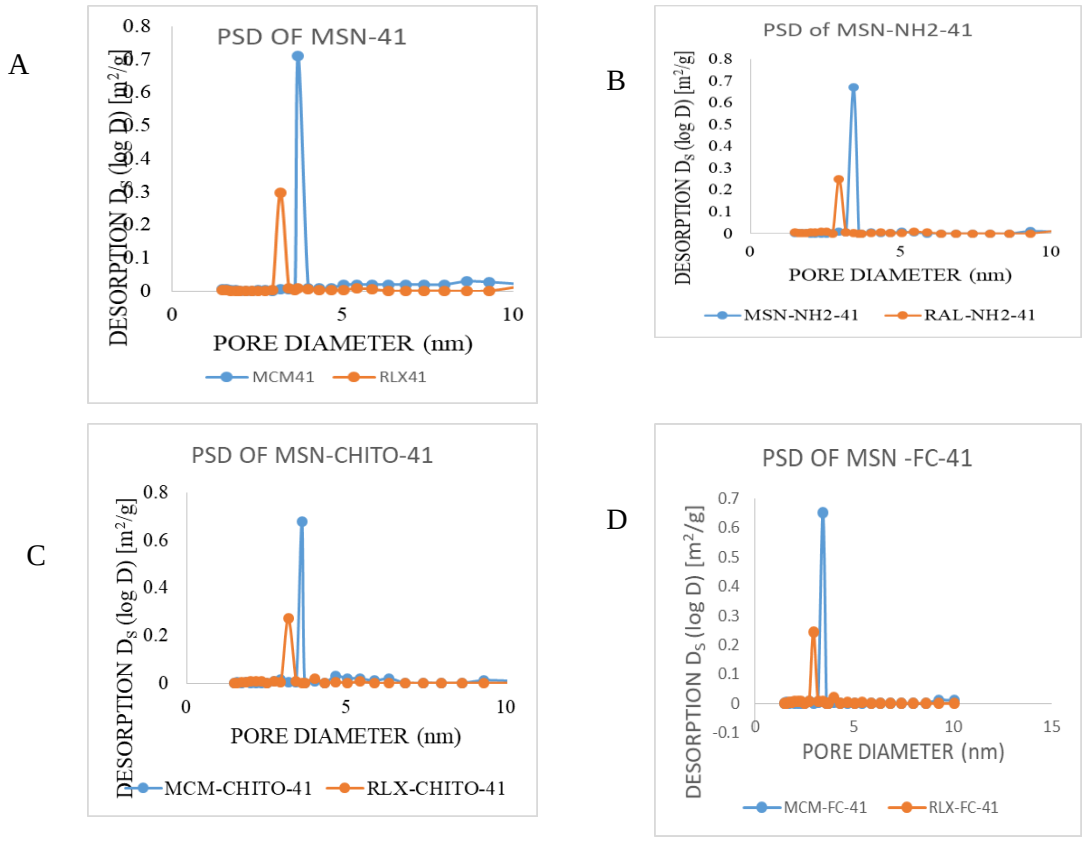

Figure 5.17: PSD graph for (A) MCM-41, (B) MCM-NH_2-41, (C) MCM-CHITO-41 and (D) MCM-FC-41

Table 5.3: BET and ZETA characteristics for bare and surface coated MCM-41

Sample name	BET surface area (m^2/g)	BJH surface area (m^2/g)	Pore size (nm)	Pore volume (cm^3/g)	Hydrodynamic size (nm)	Zeta potential (mV)
MCM-41	713.97	1141.37	3.69	0.68	96	-30.2
RLX-41	394.74	550.23	3.11	0.29	-	-16.5
MCM-NH_2-41	529.18	786.92	3.48	0.67	112	+12.6
RLX-NH_2-41	315.96	491.99	2.96	0.25	-	+25.8
MCM-CHITO-41	258.14	338.47	3.61	0.71	146	+29.4
RLX-CHITO-41	151.25	229.24	3.12	0.27	-	+41.3
MCM-FC-41	185.16	256.39	3.43	0.65	149	+30.89
RLX-FC-41	131.89	204.72	2.94	0.25	-	+40.65

A

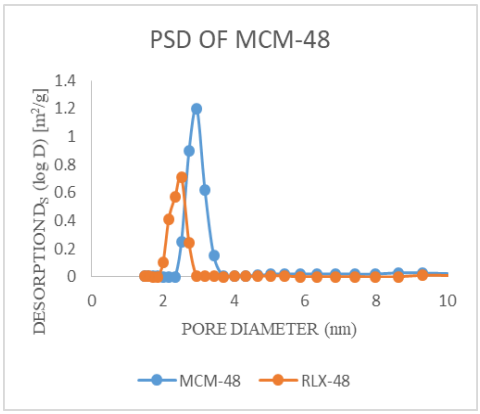

B

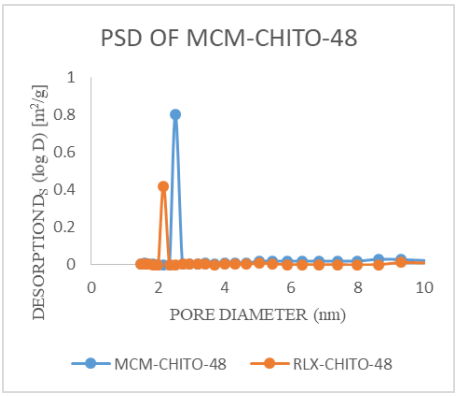

C

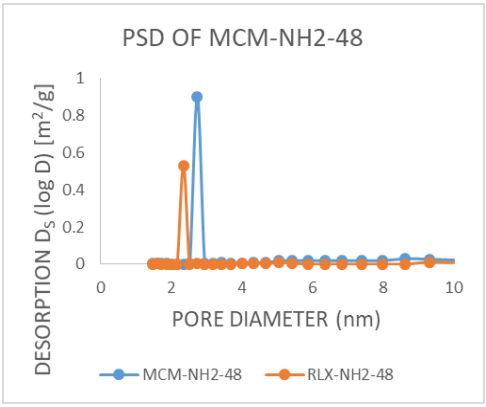

D

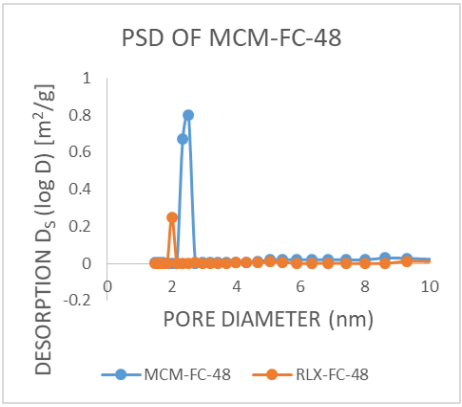

Figure 5.18: PSD graph for (A) MCM-48, (B) MCM-NH₂-48, (C) MCM-CHITO-48 and (D) MCM-FC-48

Table 5.4: BET and ZETA characteristics for bare and surface coated MCM-48

Sample name	BET surface area (m^2/g)	BJH surface area (m^2/g)	Pore size (nm)	Pore volume (cm^3/g)	Hydrodynamic size (nm)	Zeta potential (mV)
MCM-48	997.90	1465.49	2.95	1.20	91	-25.8
RLX-48	472.75	709.23	2.52	0.71	-	-12.2
MCM-NH_2-48	690.57	831.85	2.73	0.90	105	+14.9
RLX-NH_2-48	325.14	567.47	2.34	0.53	-	+28.6
MCM-CHITO-48	351.67	599.42	2.52	0.8	131	+27.12
RLX-CHITO-48	250.31	412.84	2.16	0.42	-	+34.68
MCM-FC-48	212.28	337.15	2.34	0.67	137	+31.08
RLX-FC-48	174.19	289.21	2.01	0.25	-	+41.73

5.3.1.6. DLS study:

The surface charge for the pristine MCM-41 particles remain positive due to the presence of abundant silanol group on the outer surface. The shifting of the zeta potential of MCM-41 from negative side (-30.2) to a positive value (+12.6) is due to the presence of an amine group on

the surface of MCM-NH_2-41. Whereas, in case of MCM-CHITO-41 the potential value shifted toward upper side i.e. from -30.2 mV to +29.4 exhibited surface coating with the chitosan moiety. Lastly, the values were +30.89 mV for MCM-FC-41 which demonstrated increment in the positively charged organic moieties on the external surface further confirmed a successful coating by FC conjugates. Further, it is essential to notice a constant positive shifting in zeta potential value after RLX uptake as compared to unfilled nanoparticles. This observation concludes that the RLX moiety might have positively charged surface which could be responsible in the enhancement of the potential after drug encapsulation (table 5.3). Additionally, the particle size reading was also acquired from DLS study, which revealed formation of monodispersed nanoparticles in the range of 90-150 nm with successive increment with the coating. The similar zeta potential pattern was observed for RLX free and RLX filled bare and surface coated MCM-48 nanoparticles and the outcomes are listed in the table 5.4.

5.3.1.7. SEM and TEM analysis:

The uniformity in the particle size and shape were asserted following SEM and TEM data. Figure 5.19 and figure 5.20 illustrated SEM images for bare and surface coated MCM-41 and MCM-48 nanoparticles, which displayed a uniform spherical shape of MSNs. The further idea regarding the particle size were obtained from the SEM analysis. The 2D hexagonal and 3D cubic mesoporous frameworks for MCM-41 and MCM-48 nanoparticle respectively were revealed from TEM analysis. The mesoporous skeleton was remained undisturbed even after surface coating also which could be inferred from the TEM inspection of surface decorated nanoparticles. Figure 5.21 and figure 5.22 revealed a TEM images for synthesized bare and surface modified nanoparticles for MCM-41 and MCM-48 respectively. Where, figure 5.21 is corresponding to the 2D hexagonal honeycomb assembly of MCM-41. Whereas, the 3D cubic channel observed for MCM-48 was clearly seen in the respective figure 5.22. The results demonstrated an undisturbed internal 2D hexagonal and 3D cubic skeleton even after surface modification.

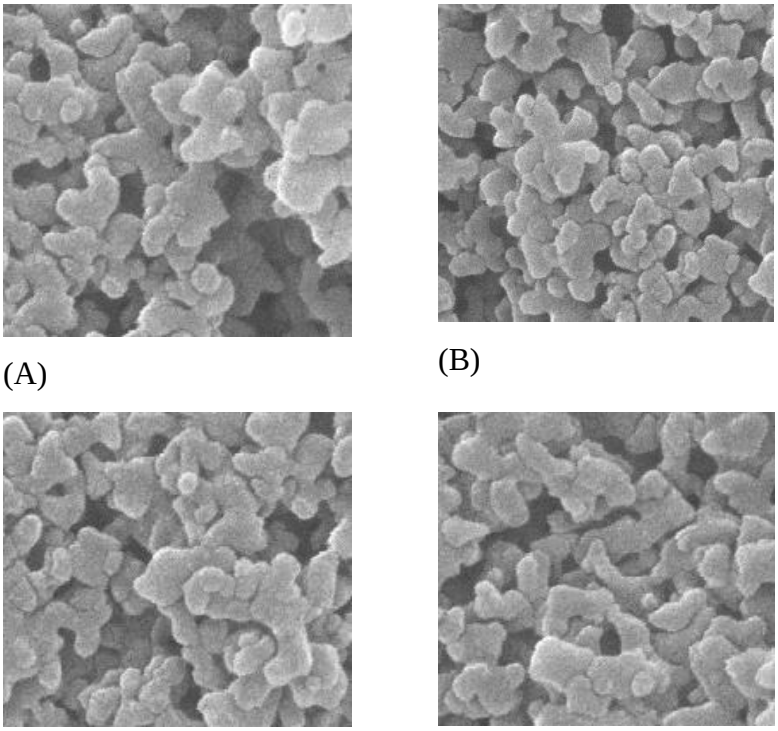

(A) (B)

(C) (D)

Figure 5.19: SEM images for (A) MCM-41, (B) MCM-NH_2-41, (C) MCM-CHITO-41 and MCM-FC-41

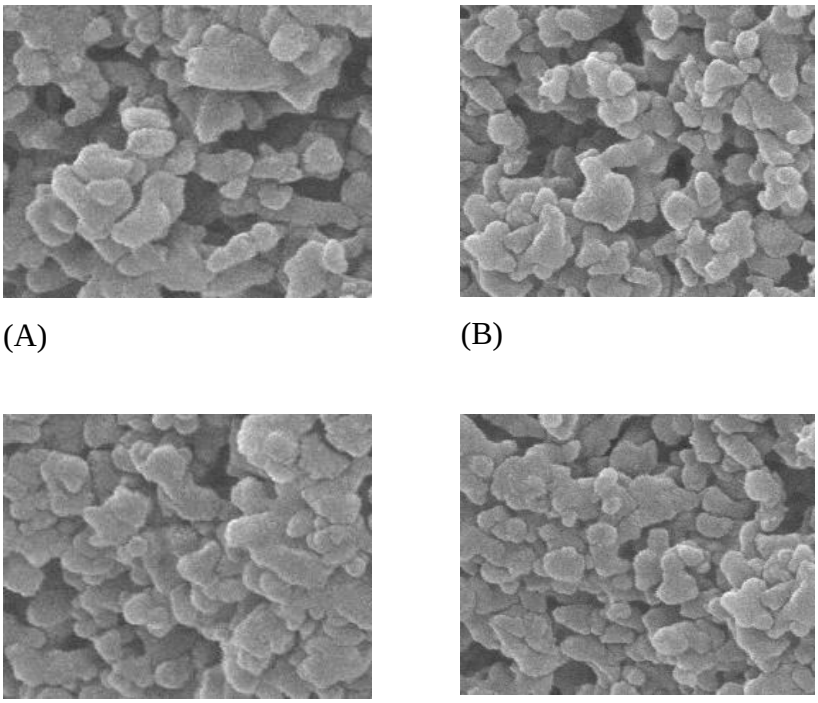

(A) (B)

(C) (D)

Figure 5.20: SEM images for (A) MCM-48, (B) MCM-NH_2-48, (C) MCM-CHITO-48 and MCM-FC-48

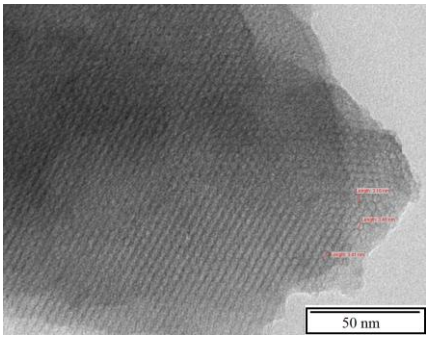

(A)

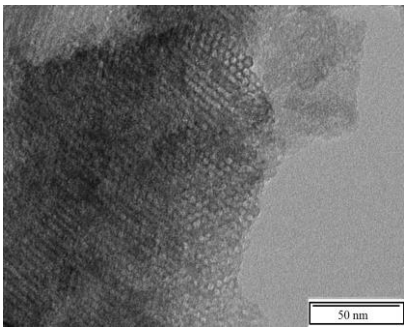

(B)

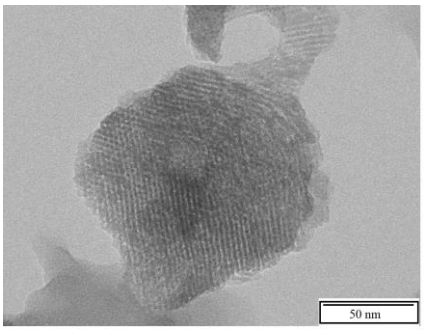

(C)

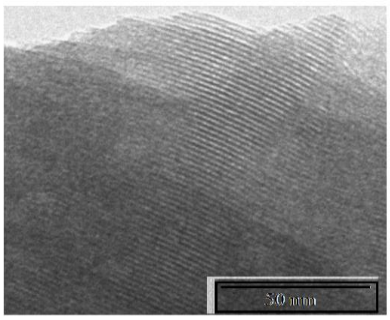

(D)

Figure 5.21: TEM images for (A) MCM-41, (B) MCM-NH_2-41, (C) MCM-CHITO-41 and MCM-FC-41

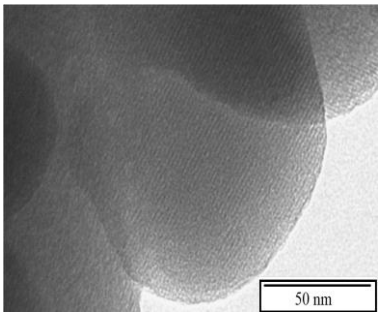

(A)

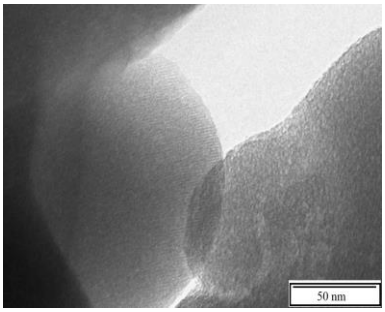

(B)

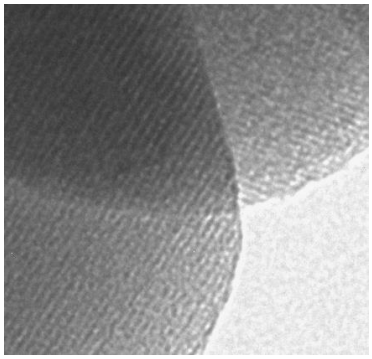

(C)

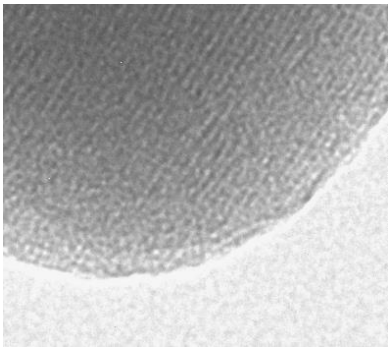

(D)

Figure 5.22: TEM images for (A) MCM-48, (B) MCM-NH_2-48, (C) MCM-CHITO-48 and MCM-FC-48

5.3.2. Estimation of %loading efficiency and entrapment efficiency:

The RLX loaded nanoparticles were prepared using a novel immersion evaporation technique. As being a hydrophobic drug, RLX is having maximum solubility in organic solvent especially in MeOH. Therefore, during the drug loading, RLX was dissolved in MeOH and in this solubilized form, active drug molecule diffuses inside the mesopores through the capillaries and after solvent removal, drug remains entrapped inside the pores. Though confirmation of uptake by nanoparticles were accomplished through aforementioned different techniques, the extent of loading and entrapment for carrier and RLX respectively were still left to be determined. This investigation was conducted performing UV and TGA analysis of RLX engulfed nanoparticles. Information collected from both the techniques were complementary to each other as summarized in table 5.5. The TGA curve of RLX displayed an expeditious fall initiated at near 200 ºC and lasted upto 300 ºC. This could be due to thermal decomposition of drug moiety. The RLX thermogram showed complete decomposition of pure drug moiety with the 100 %weight loss. Further the %loading efficiency was calculated from the weight loss of the RLX assembled in nanosystem. Pictorial representation of TGA graphs demonstrating the %loading efficiency is portrayed in following figures. Figure 5.23 and 5.24 is corresponded to %loading graph of bare and surface coated MCM-41 and MCM-48 types of nanosystems. Results exhibited extensive loading capacity of bare nanoparticles to entrap the positively charged RLX as these nanosystems are having negatively charged surface. Furthermore, the loading capacity declined for MCM-NH_2-41, MCM-CHITO-41 and MCM-FC-41 and also for MCM-NH_2-48, MCM-CHITO-48 and MCM-FC-48 which could be attributed to its positively charged surface.

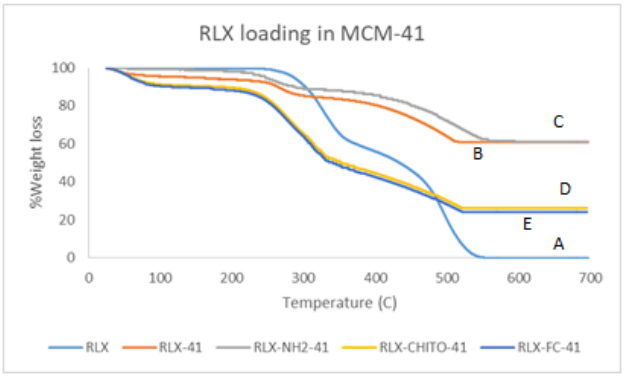

Figure 5.23: TGA thermogram of (A) RLX, (B) RLX-41, (C) RLX-NH_2-41 (D) RLX-CHITO-41 and (E) RLX-FC-41

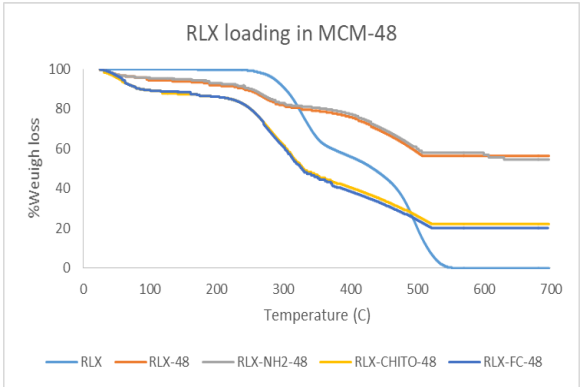

Figure 5.24: TGA thermogram of (A) RLX, (B) RLX-48, (C) RLX-NH_2-48 (D) RLX-CHITO-48 and (E) RLX-FC-48

Table 5.5: %Loading and %entrapment efficiency data of RLX

Sample	Drug:Carrier ratio	% Loading efficiency		% Entrapment efficiency
		UV	TGA	
RLX-41	1:1.5	35.53	34.87	87.54
RLX-NH_2-41	1:1.5	32.15	31.89	80.37
RLX-CHITO-41	1:1.5	34.96	33.57	86.81
RLX-FC-41	1:1.5	31.66	30.28	79.15
RLX-48	1:1.5	39.45	38.87	97.55
RLX-NH_2-48	1:1.5	36.48	35.69	88.86
RLX-CHITO-48	1:1.5	35.12	34.53	86.32
RLX-FC-48	1:1.5	34.91	34.04	85.11

5.3.3. %Grafting of different surface modifying agents

The Ninhydrin colorimetric assay was performed and absorbance of Ninhydrin-primary amine complex was taken into consideration for the %amine grafting calculation. Colorimetric analysis of MCM-NH_2-41 and MCM-NH_2-48 at 590 nm showed 4.20% and 4.93% amine decoration on the surface of the plain MCM-41 and MCM-48 respectively. The results were calculated applying equation 5.1-5.3.

TGA results are represented in terms of temperature dependent weight loss (31). Wherein the TGA graph was divided into two distinctive temperature range regions. The first region comprises of region of weight change between 20-150 °C. The weight loss occurred over this range of temperature could be solely accredited to the thermal desorption of surface water adsorbed physically over the silica surface. On the other hand, the second region comprised of weight change beyond 150°C temperature. A comparative flat TGA curve represents a negligible weight loss at the higher temperature. The minor change in the weight could be assigned to silanol condensation followed by siloxane bond formation (32). All the MSNs exhibited outstanding stability within the studied temperature range. Although the TGA curve for surface functionalized nanoparticles was easily distinguishable from that of bare silica thermogram especially in the second region of weight loss due to loss or decomposition of grafted moiety takes place beyond 150 ºC. The larger is the percentage weight loss, the higher would be extend of surface functionalization (33). Equations 4-6 were taken into consideration for the %amine grafting calculation by TGA and the results were in accordance with the

outcome obtained from Ninhydrin colorimetric assay (figure 5.25 and 5.26). further the figure of %grafting for MCM-41 and MCM-48 is listed in table 5.6.

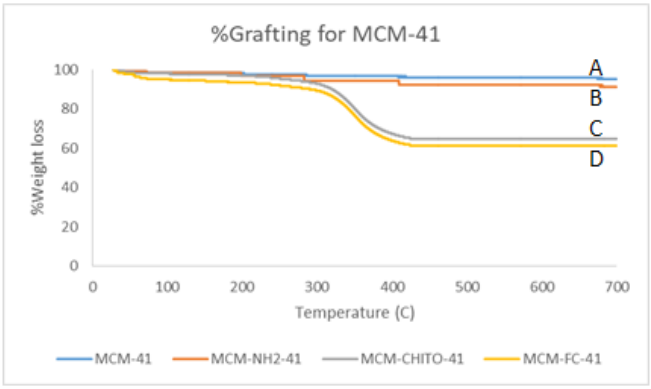

Figure 5.25: TGA thermogram showing %grafting in MCM-41 nanoparticle

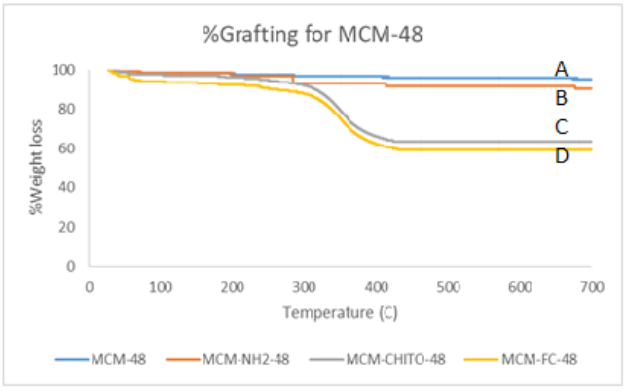

Figure 5.26: TGA thermogram showing %grafting in MCM-48 nanoparticle

Table 5.6: %Weight grafting results

Sample Name	A_m (mol/g)	A_n (molecule/nm^2)	%W	
			Ninhydrin	TGA
MCM-NH_2-41	$0.19*10^{-3}$	0.20	4.20	4.01
MCM-CHITO-41	-	-	-	28.51
MCM-FC-41	-	-	-	22.87
MCM-NH_2-48	$0.22*10^{-3}$	0.12	4.93	4.87
MCM-CHITO-48	-	-	-	29.57
MCM-FC-48	-	-	-	25.68

Besides this, the elemental detection of different moieties present in pristine and amine modified nanoparticles outcomes revealed presence of Si and Oxygen elements in the bare MSNs whereas, the extra peak due to nitrogen and carbon encountered in the MCM-NH_2-41, MCM-CHITO-41 and MCM-FC-41 (figure 5.27) as well for MCM-NH_2-48, MCM-CHITO-48 and MCM-FC-48 (figure 5.28) confirmed the success of amine, chitosan and FC conjugate coating on the exterior.

(A)

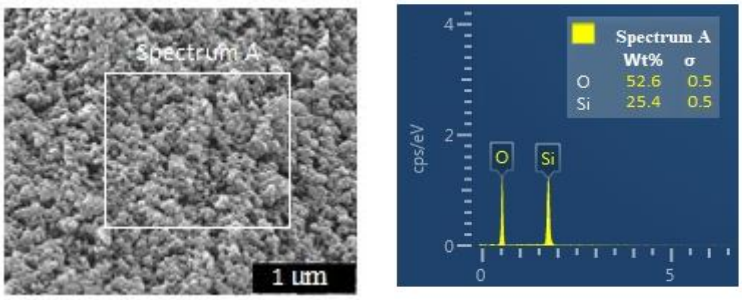

(B)

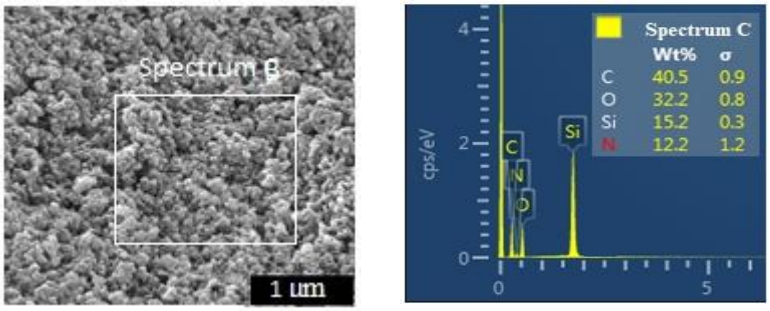

(C)

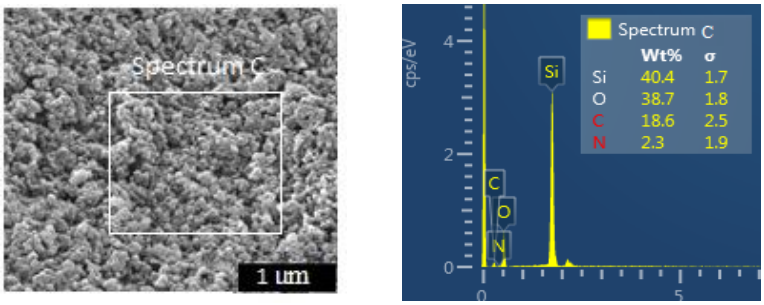

(D)

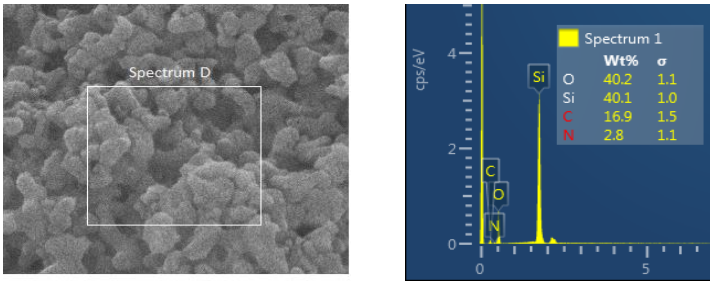

Figure 5.27: SEM-EDX images for (A) MCM-41, (B) MCM-NH_2 -41 (C) MCM-CHITO-41 and (D) MCM-FC-41

(A)

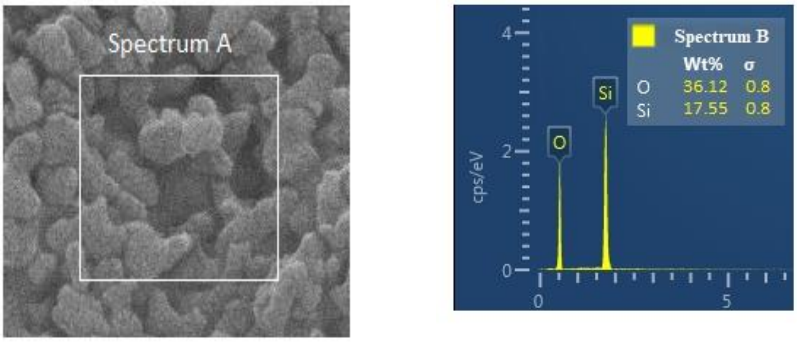

(B)

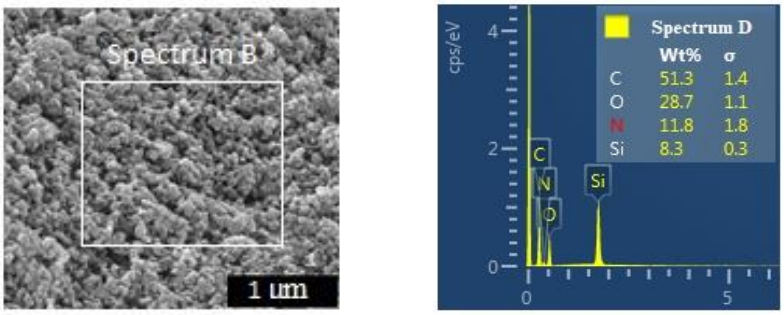

(C)

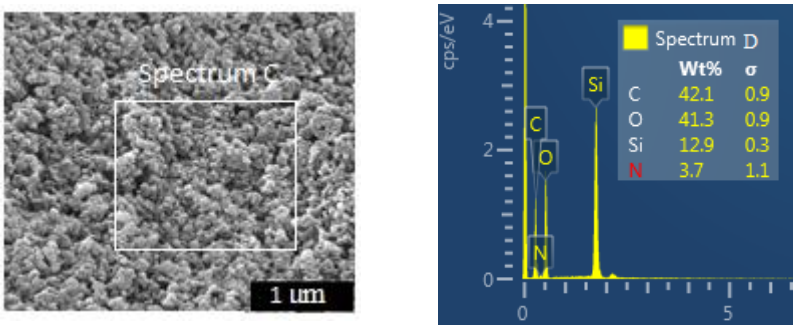

(D)

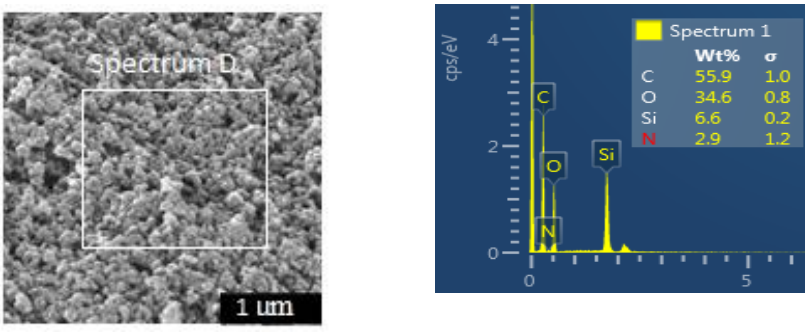

Figure 5.28: SEM-EDX images for (A) MCM-48, (B) MCM-NH_2 -48 (C) MCM-CHITO-48 and (D) MCM-FC-48

5.3.4. Formulation development:

The formulated RLX tablets were assessed for hardness, disintegration time, friability, weight variation test and drug content and result for each parameter are recorded in table 5.7. Hardness data for both formulations was ranging from 3.8 to 4.4 kg/cm^2 which says that the tablet hardness was sufficient enough to withstand the external pressure. Tablet prepared using standard excipient showed disintegration time of 2±0.2 min, friability of below 1% and 97.12-101.86 %drug content values were within the standard limit for both the tablets. Formulated tablets were evaluated for their hardness, disintegration time, friability, weight variation test and drug content parameters and the results were found to be within the limit as per the IP criteria.

Table 5.7: Evaluation of prepared RLX-MCM-41 and RLX-MCM-48 tablet

Parameters	**RLX-41**	**RLX- 48**	**RLX-NH_2-41**	**RLX-NH_2-48**
Hardness	3.8-4.2 kg/cm^2	3.9-4.4 kg/cm^2	3.9-4.3 kg/cm^2	3.9-4.3 kg/cm^2
Disintegration Time	<2 min	<2 min	<2 min	<2 min
Friability	Below 1%	Below 1%	Below 1%	Below 1%
Weight variation	305.62±3.53789	306.85±2.84	304.15±2.47	305.25±2.44
% Drug content	97.12-101.56%	98.56-101.88%	98.99-101.37%	98.34-101.67%

5.3.5. In vitro dissolution study release study:

The punched tablets of RLX-41, RLX-48, RLX-NH_2-41 and RLX-NH_2-48 were taken further to conduct dissolution study. The *in vitro* release study exhibited higher RLX release from each four formulation in SGF media supplemented with 0.1% polysorbate 80 (pH 1.8) in contrast to SIF media enriched with 0.1% polysorbate 80 (pH 6.8). Superior release of RLX was obtained from RLX-48 nanoparticles compare to RLX-41. Where the former formulation showed burst release of drug within initial 15 min and displayed complete release within 45 min in SGF media. Whereas, the latter formulation *i.e.* MCM-41 required around 75 min for the complete drug release from the 2D hexagonal structure. The comparative study of synthesized formulation *i.e.* MCM-41 and MCM-48 with marketed formulation and plain RLX divulged superiority of synthesized nanoparticles over plain API to a greater extent and over marketed formulation to a lesser extent. It took around 120 min for complete RLX release from MF which was higher than the time taken by MCM-41 and MCM-48 to empty the RLX. On

the other side, it was only 26% cumulative RLX release from the plain RLX in SGF media (figure 5.29).

Furthermore, the amine modified nanocarriers demonstrated slower release of RLX with respect to RLX release from their respective pristine nanoframework. The reason of hindering the drug release could be attributed to amine decoration of the external surface. The release of RLX was hindered in SIF media also. But the release of RLX from both the nanosystem were still superior compared to pure API and MF. Results unveiled 85% and 73% of RLX release from MCM-48 and MCM-41 respectively, whereas the figure was lesser for MF and plain RLX. The RLX-NH_2-41 and RLX-NH_2-48 displayed hindered release in SIF media also and again the reason would be the same *i.e.* functionalization might have significant impact on the RLX release. Here the result obtained were performed by taking n=6 dissolution set.

Figure 5.29D-G represented drug release behaviour in bioreleavant media *viz.*, FaSSGF, FeSSGF, FaSSIF-V2 and FeSSIF. As observed earlier, complete release achieved in gastric pH with contrast to intestinal pH. RLX-48 demonstrated almost complete release in FaSSGF and FeSSGF as compared to RLX-41 and MF which imparted to 82% and 65% release respectively in 60 min. Similarly, RLX-48, RLX-41 and MF provided approximately 82%, 60% and a 50% release in FaSSIF-V2 and FeSSIF in 60 min. Thus, the resemblance in the release pattern in the fasted and fed conditions lead to a conclusion that RLX release is independent of the presence of food. The similar conclusion was drawn for aminated nanicarriers also.

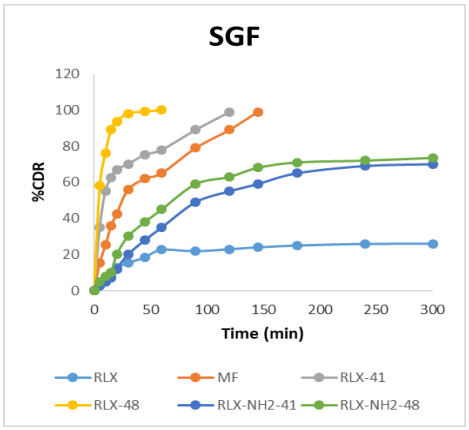

(A)

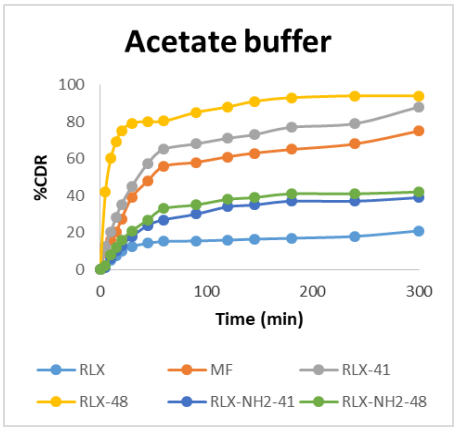

(B)

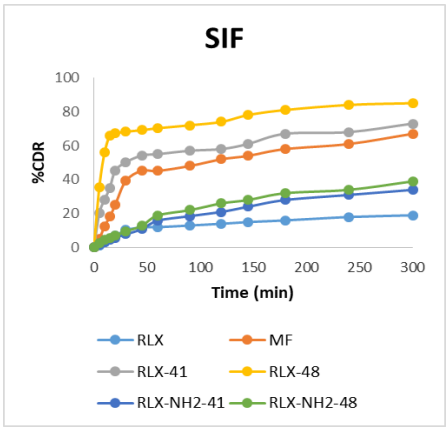

(C)

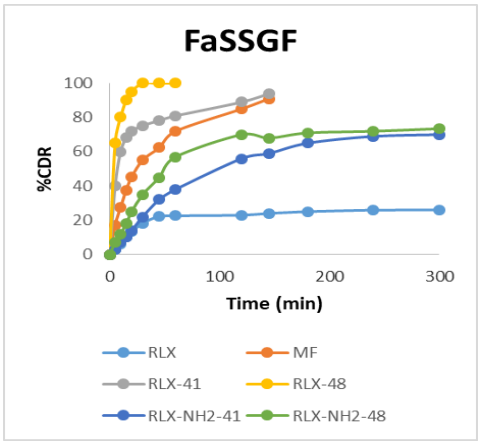

(D)

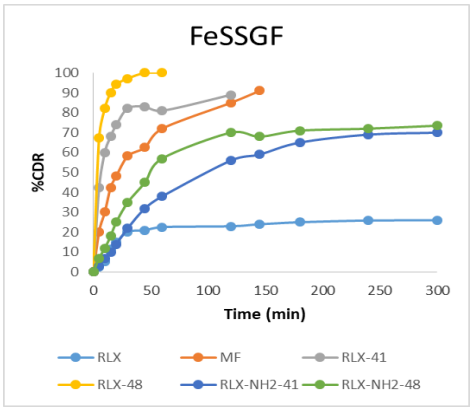

(E)

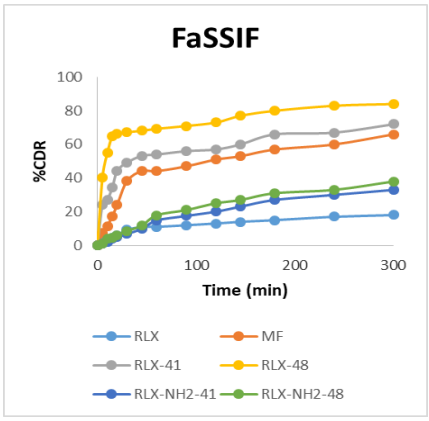

(F)

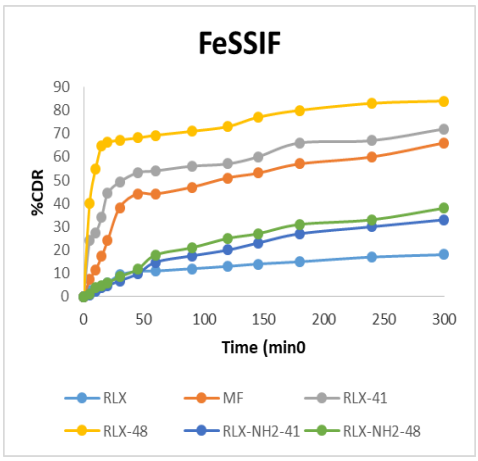

(G)

Figure 5.29. *In vitro* release study of drug loaded nanoparticles in different dissolution media

5.3.6. In vitro diffusion study release study:

In vitro study was carried out in PBS solution at three different pH *viz.*, at 5.6, 6.8 and 7.4 representing release behaviour of RLX loaded MSNs in varied pH. Figure 5.30 depicts the release pattern of plain RLX, RLX-41, RLX-NH_2-41, RLX-CHITO-41 and RLX-FC-41 in PBS solution. Results demonstrated rapid release of RLX at acidic pH (pH 5.6). In contrast, release of RLX was very slow at pH 7.4. A comprehensive pH responsive study demonstrated 10.5±0.15%, 82.6±1.89%, 68.8±1.44% and 84.2±0.98% cumulative RLX release from plain RLX, RLX-41, RLX-NH_2-41 and RLX-CHITO-41 in PBS 5.6 pH. Furthermore, it was 9.9%±2.16, 80.2±1.77%, 64.1±1.05 and 65.7±0.62% at pH 6.8 and 9.5±1.52%, 79.9±1.69%, 62.8±1.34% and 57.5±1.01% at pH 7.4 respectively for RLX, RLX-41, RLX-NH_2-41 and RLX-CHITO-41.

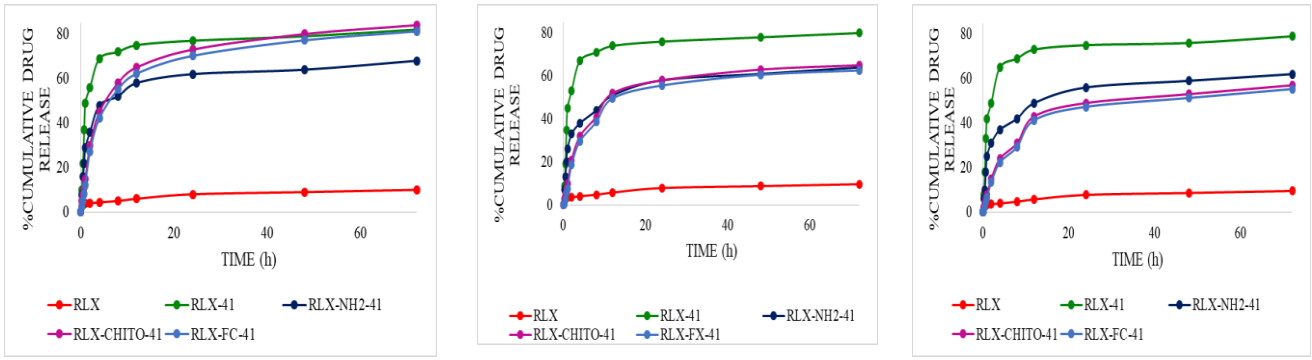

(A) (B) (C)

Figure 5.30: *In vitro* diffusion study in PBS solution at (A) pH: 5.6, (B) pH 6.8 and (C) pH 7.4

Figure 5.31 depicts the release pattern of plain RLX, RLX-48, RLX-NH_2-48, RLX-CHITO-48 and RLX-FC-48 in PBS solution. Results demonstrated rapid release of RLX at acidic pH (pH 5.6) from RLX-CHITO-48. In contrast, release of RLX was very slow at pH 7.4. A comprehensive pH responsive study demonstrated 10.21±0.51%, 86.91±1.55%, 75.9±1.48% 89.53±0.75% and 98.66±0.88% cumulative RLX release from plain RLX, RLX-48, RLX-NH_2-48, RLX-CHITO-48 and RLX-FC-48 in PBS 5.6 pH. Furthermore, it was 9.73±0.82%, 84.14±0.99%, 69.7±0.34%, 68.5±0.71% and 65.88±0.83% at pH 6.8 and 9.53%±1.56, 82.2±1.77%, 68.1±0.15%, 66.7±0.82% and 64.3±0.15% at pH 7.4 respectively for RLX, RLX-48, RLX-NH_2-48, RLX-CHITO-48 and RLX-FC-48.

(A) (B) (C)

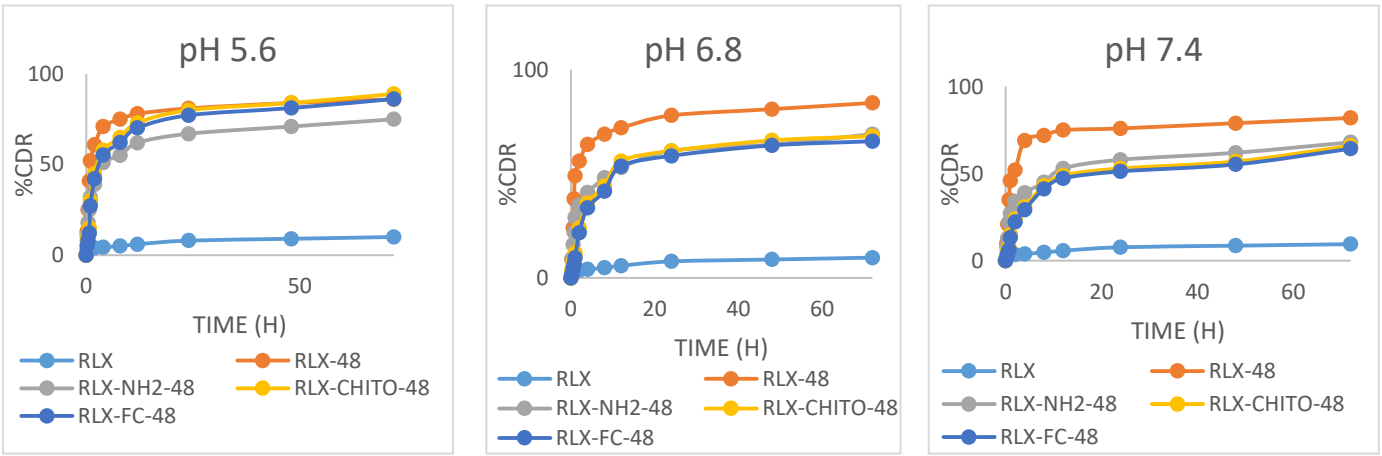

Figure 5.31: *In vitro* diffusion study of RLX encapsulated in MCM-48 in PBS solution at (A) pH: 5.6, (B) pH 6.8 and (C) pH 7.4

5.3.7. In vitro cytotoxicity study on Caco-2 cell line for oral formulation:

MTT assay was performed to screen out the maximum concentration of RLX loaded nanoparticle up to which they could be utilized to carry out the *in vitro* permeability study. Herein, the MTT assay was performed for drug free nanoparticles and drug loaded nanoparticles on the received Caco-2 cell line incubating for 4 h. The result demonstrated the safe nature of plain and RLX loaded nanoparticles toward Caco-2 cells in the concentration range of 10-100 µM. The %relative viability was >98.57±0.71% for drug free bare and amine coated nanoparticles (figure 5.32A). Whereas the %relative viability was >95.20±0.74% for RLX-41, RLX-48, RLX-NH_2-41 and RLX-NH_2-48 as shown in figure 5.32B.

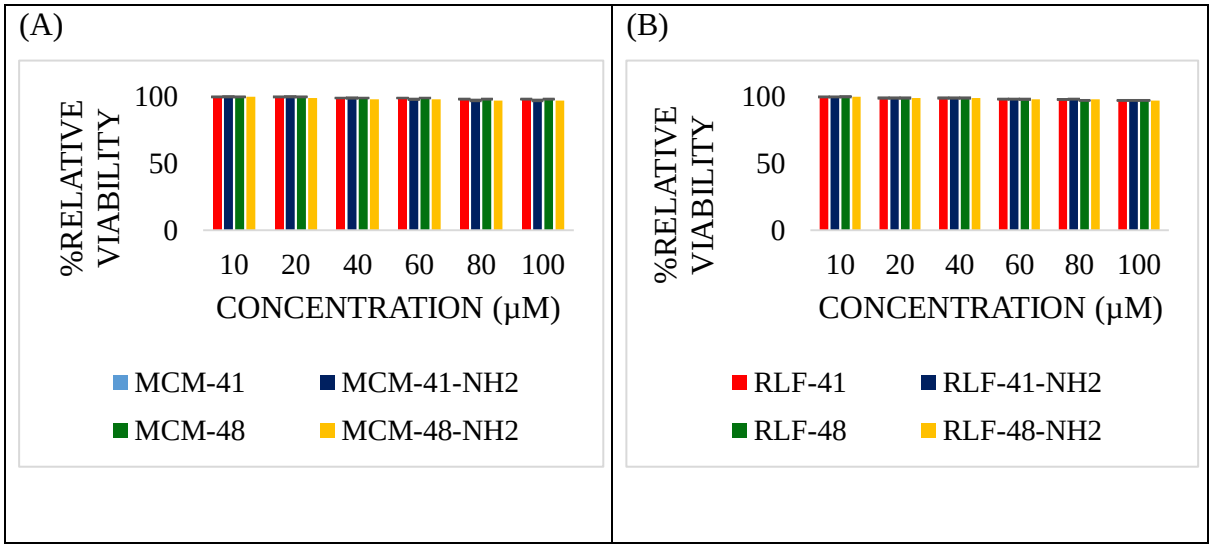

Figure 5.32: Cell viability graph for (A) drug free and (B) drug filled bare and amine coated nanoparticles

5.3.8. In vitro cytotoxicity study on MCF-7 cell line for parenteral formulation:

The concentration and time dependent cell cytotoxicity study in the range of 0.1-100 µM concertation for 24 and 72 h respectively was performed for MCM-41, MCM-NH_2-41, MCM-CHITO-41, MCM-FC-41 and MCM-48, MCM-NH_2-48, MCM-CHITO-48, MCM-FC-48. The investigation outcome revealed 98.20 ± 0.88, 97.30 ± 0.57, 96.40 ± 1.02 and 96.15 ± 0.69 %relative viability for MCM-41, MCM-NH_2-41, MCM-CHITO-41 and MCM-FC-41 respectively for 24 h. Whereas, the cytotoxicity study result of 72 h revealed 97.25 ± 0.46 and 94.68 ± 0.12% relative cell viability for MCM-41, MCM-NH_2-41, MCM-CHITO-41 and MCM-FC-41 respectively. On the other hand, the results for MCM-48, MCM-NH_2-48 and MCM-CHITO-48 demonstrated 99.10 ± 0.28, 98.20 ± 1.09, 96.40 ± 0.91 and 96.15 ± 0.71

%relative viability after 24 h and 97.30 ± 0.65, 96.59 ± 0.63, 94.51 ± 0.29 and 96.40 ± 0.33 %relative viability after 72 h respectively (figure 5.33).

Besides this the similar study was also carried out for RLX, RLX-41, RLX-NH_2-41, RLX-CHITO-41, RLX-FC-41 and RLX-48, RLX-NH_2-48, RLX-CHITO-48, RLX-FC-48 in the range of 1-8 µM concertation for 24 and 72 h respectively. The result showed 78.89 ± 1.22, 42.58 ± 0.98, 62.56±0.36, 46.77 ± 1.08 and 39.58±0.47 %relative viability and 70.82 ± 1.38, 25.67 ± 1.55, 31.84±0.74, 19.05 ± 1.04 and 14.87±0.54 %relative viability after an incubation time of 24h and72 h respectively for the MCM-41 type of carriers. Whereas the result were showing 78.89 ± 1.22, 40.91 ± 0.68, 58.56±0.34, 40.32 ± 0.78 and 34.27±0.77 %relative viability and 70.82 ± 1.38, 23.44± 0.95, 28.33±0.14, 15.85 ± 1.25 and 8.78±1.27 %relative viability for RLX-48, RLX-NH_2-48, RLX-CHITO-48 and RLX-FC-48 after 24h and 72h respectively (figure 5.34). Thus, it could be stated that the degree of cytotoxicity is purely attributed to drug moiety encapsulated in the MSNs. Additionally, the cytotoxicity result proved a greater cytotoxic potential of MCM-48 type of nanoparticles. Further the IC50 obtained for each formulation is mentioned in below table 5.8 and table 5.9.

(A)

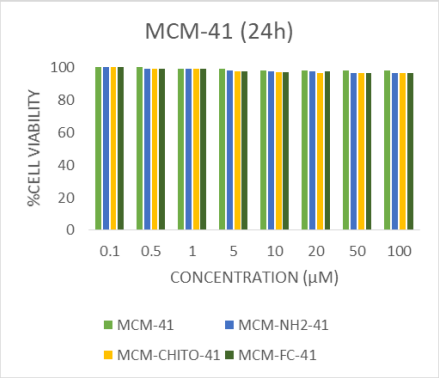

(B)

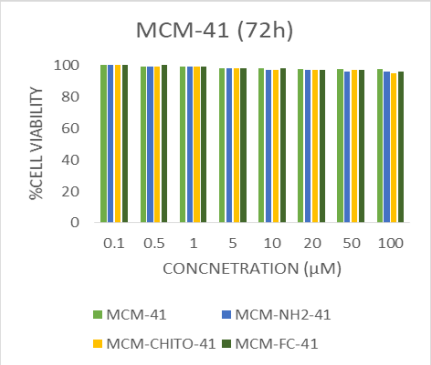

(C)

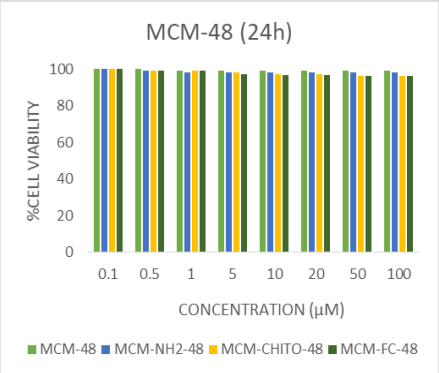

(D)

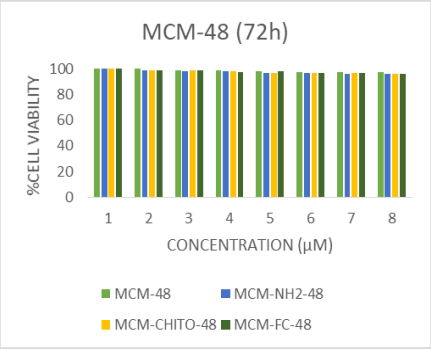

Figure 5.33: Cell viability graph for drug free MCM-41 type of nanoparticles after (A) 24h and (B) 72h; and for MCM-48 type of nanoparticles after (C) 24h and (D) 72h

(A)

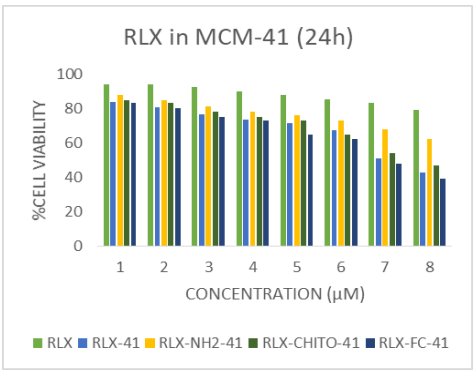

(B)

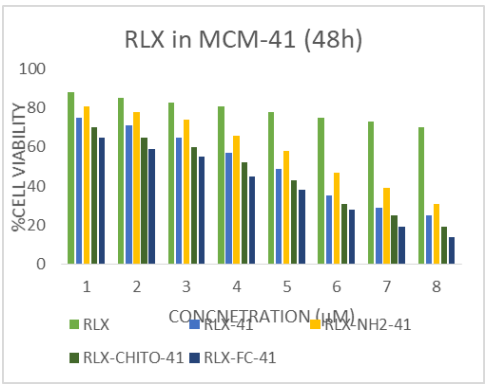

(C)

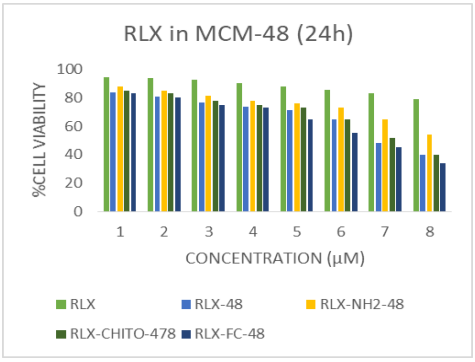

(D)

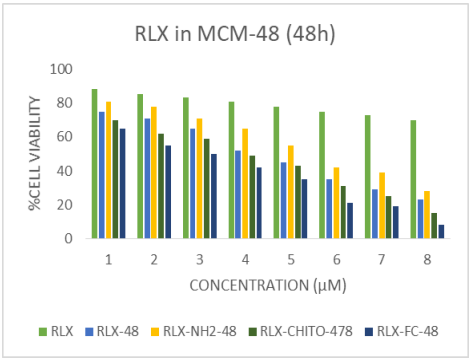

Figure 5.34: Cell viability graph for drug loaded MCM-41 type of nanoparticles after (A) 24h and (B) 72h; and for MCM-48 type of nanoparticles after (C) 24h and (D) 72h

Table 5.8: IC_{50} values for RLX nanoparticles encapsulated in MCM-41

Time (h)	Concentration with respect to IC_{50} (µM)*				
	RLX	RLX-41	RLX-NH_2-41	RLX-CHITO-41	RLX-FC-41
24	>8	7.16±0.12	>8	7.53±0.56	6.8±0.47
72	>8	4.86±0.75	5.67±0.23	4.27±0.89	3.5±0.27

* The study was conducted in three replicates and results were displayed in mean±S.D.

Table 5.9: IC_{50} values for RLX nanoparticles encapsulated in MCM-48

Time (h)	Concentration with respect to IC_{50} (µM)*				
	RLX	RLX-48	RLX-NH_2-48	RLX-CHITO-48	RLX-FC-48
24	>8	6.89±0.42	>8	7.12±0.91	6.52±0.83
72	>8	4.21±0.11	5.34±0.92	3.92±0.19	3.01±0.71

* The study was conducted in three replicates and results were displayed in mean±S.D.

5.3.9. In vitro permeability study for oral formulation:

From the MTT cytotoxicity study RLX concentration was selected to be 100 µg/mL concentration was considered to be a safe concentration as it was having no negative influence on the Caco-2 cell viability. A Transport experiment was performed for RLX release evaluation from apical to basal compartment transportation. Wherein, the P_{app} value was estimated at the end of 24 h calculated individually for different formulation as listed in the table 5.10. The data revealed nearly 4.31 and 5.31-fold increment in the permeability for RLX-41 and RLX-48 respectively, whereas the coefficient value was declined for RLX-NH_2-41 and RLX-NH_2-48 with respect to bare nanoparticle but these were still greater as compared to permeability of pure RLX *i.e.* 2.77 and 3.16 respectively. Therefore, the permeability results unveiled enhanced permeability of RLX by designing and encapsulating them into mesoporous nanosystem.

Table 5.10. Permeability study of formulated nanoparticles

TIME (min)	RLX	RLX-41	RLX-48	RLX-NH_2-41	RLX-NH_2-48
30	0.71	4.99	5.31	2.11	3.88
60	.66	8.46	10.77	5.32	7.31
90	3.94	14.34	16.24	5.66	10.56
120	5.93	19.83	23.84	12.24	15.39
180	7.11	25.66	35.19	19.43	22.47
240	9.87	39.14	48.56	24.18	27.35
300	11.56	49.75	61.47	31.34	35.81
dQ/dt	0.0385	0.1658	0.2049	0.1045	0.1193
P_{app}	$2.046*10^{-2}$	$8.805*10^{-2}$	$1.087*10^{-1}$	$5.54*10^{-2}$	$6.33*10^{-2}$

5.3.10. Cellular uptake by confocal microscopy:

The FITC labelled MSNs were visualized under confocal microscope. The images demonstrated a relatively higher uptake of MCM-CHITO-41 and MCM-FC-41 with respect to FA+MCM-FC-41 after 24h. Figure 5.35 demonstrated a blue colour after staining with DAPI. When the MCF-7 cells are incubated with the FITC labelled chitosan coated nanoparticles, it showed a strong green fluorescence surrounding the nuclei, indicates a successful internalization of chitosan and chitosan-folate coated nanoparticles. Whereas the FITC labelled pristine nanoparticle showed weaker fluorescence with respect to surface coated nanoparticles. This outcome states the relatively lower efficiency of uncoated nanoparticle for the target side. Furthermore, the remarkable and intense green fluorescence for MCM-FC-41 as compared to MCM-CHITO-41 revealed higher targeting efficiency by receptor based targeted delivery system. The similar results were obtained for MCM-48 types of nanoparticles (figure 5.36).

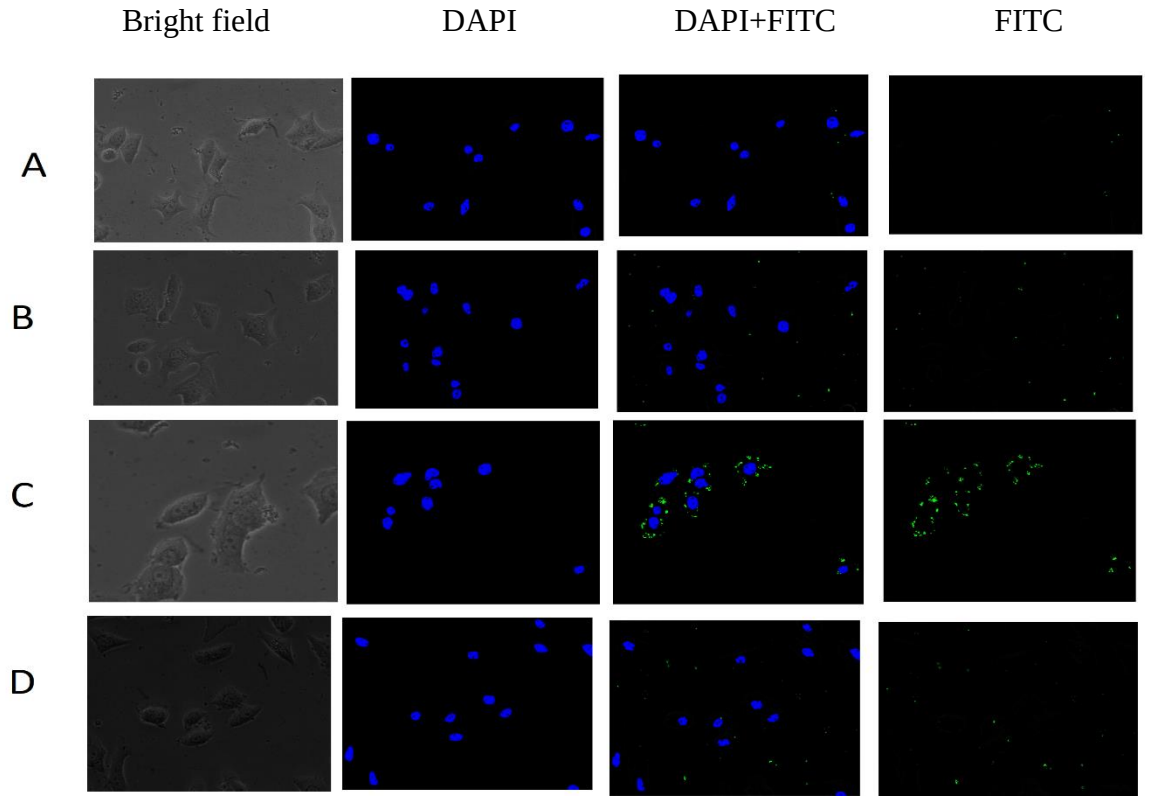

Figure 5.35. Confocal microscopic images of cellular uptake of FITC labelled MSNs (green) in MCF-7 cell line with DAPI nuclear staining(blue) for (A) MCM-NH_2-41, (B) MCM-CHITO-41, (C) MCM-FC-41 and (D) FA+MCM-FC-41

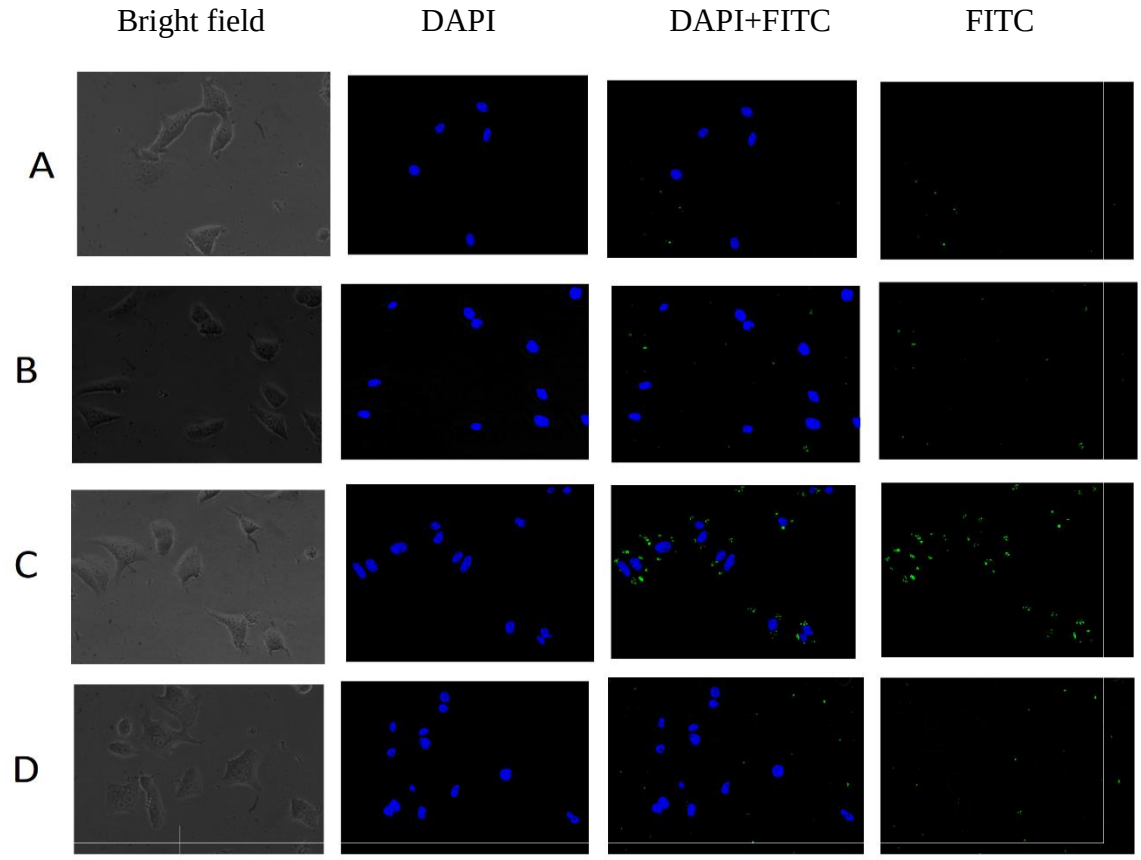

Figure 5.36. Confocal microscopic images of cellular uptake of FITC labelled MSNs (green) in MCF-7 cell line with DAPI nuclear staining(blue) for (A) MCM-NH2-48, (B) MCM-CHITO-48, (C) MCM-FC-48 and (D) FA+MCM-FC-48

5.3.11. Cellular uptake by FACS

To provide a quantitative comparison, the cellular uptake performance of aminated and surface coated nanoparticles in MCF-7 was further studied by FACS analysis. After treating MCF-7 cells with FITC labelled CHITO-MSNs and FC-MSNs for 24 h, the FITC signal emitted from the cells were very strong (Figure. 5.37 and 5.38), indicating a high cellular uptake of CHITO-MSNs and FC-MSNs. In contrast, the mean intensity of FITC from the cells incubated with FITC labelled MSNs without surface modification is only 23.44% and 26.51% respectively for MCM-NH_2-41 and MCM-NH_2-48. Moreover, FITC labelled MCM-CHITO-41 and MCM-CHITO-48 showed 67.45% and 71.39% uptake by MCF-7 cells respectively. Whereas, MCM-FC-41 and MCM-FC-48 showed higher cellular uptake *i.e.* 82.79% and 85.22%. To further confirm the specific interaction of FC-MSNs with MCF-7 cells, free FA (10 mg/mL) was added prior to the addition of FITC labelled FC-MSNs in the cell culture medium. The FITC signal intensity decreases by 45% and 49% compared to the FITC labelled MCM-FC-41 and MCM-FC-48 respectively, suggesting that the interaction between FA and FC-MSNs and the subsequent folate receptor-mediated endocytosis has been weakened due to the competition of free FA. The above results have confirmed that FC-MSNs can target folate over-expressing MCF-7 cancer cells via the FA receptor-mediated endocytosis pathway and show an improved endocytosis performance compared to the unmodified MSNs. The FACS results provide a quantitative comparison, which is consistent with the confocal microscopy observations (Fig. 5.37 and 5.38A-C).

(I) (II) (III)

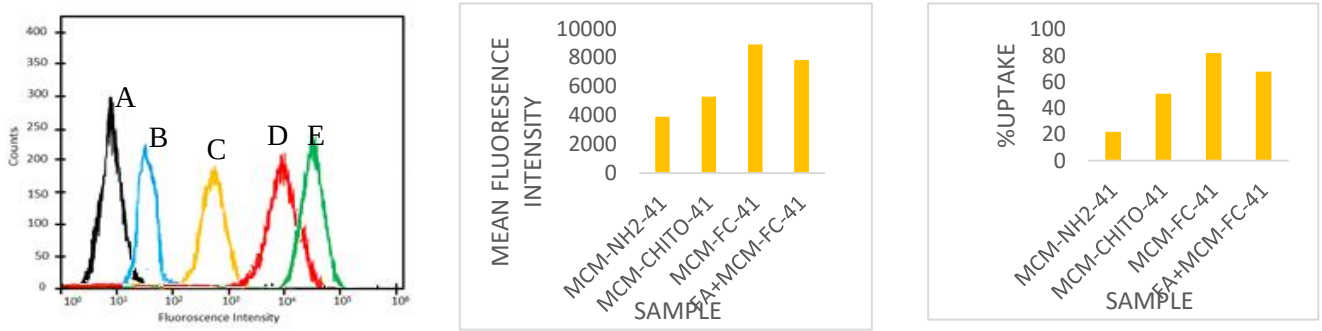

Figure 5.37: (I) Flow cytometric (II) mean fluorescence intensity and (III) %uptake data for synthesized nanoparticles

*(A) untreated cells (control), (B) MCM-NH_2-41, (C) MCM-CHITO-41, (D) FA+MCM-FC-41and (E) MCM-FC-41

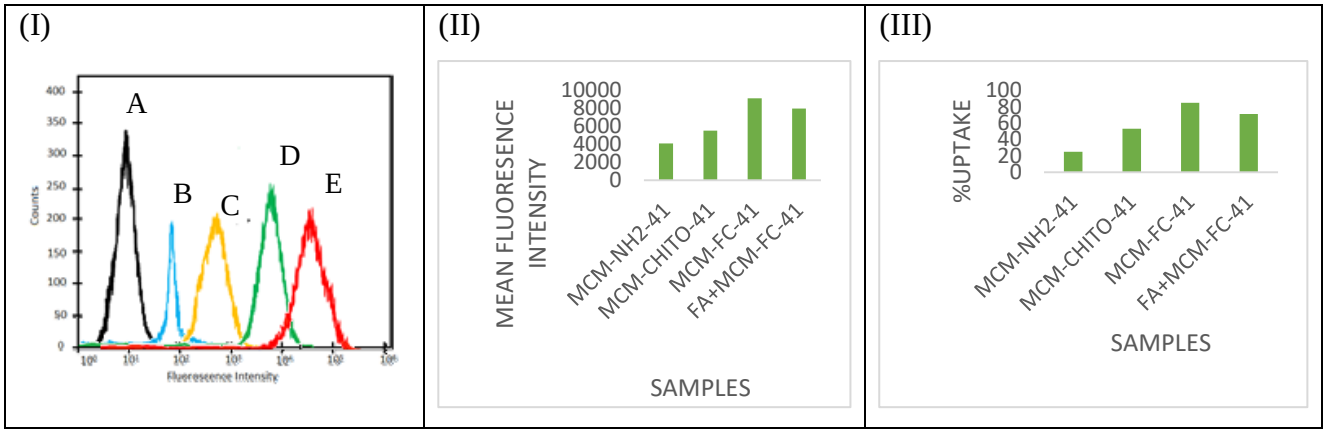

Figure 5.38: (I) Flow cytometric (II) mean fluorescence intensity and (III) %uptake data for synthesized nanoparticles

*(A) untreated cells (control), (B) MCM-NH_2-48, (C) MCM-CHITO-48, (D) FA+MCM-FC-48 and (E) MCM-FC-48

5.3.12. Apoptosis assay:

The death mechanisms were adjudged by FACS protocol using Annexin V-FITC apoptosis detection kit. The cells were treated with RLX, RLX-NH_2-41and RLX-FC-41. For MCF-7 cells, early apoptosis was observed as 5.61%, 12.89% and 56.93% in cells treated with RLX, RLX-NH_2-41 and RLX-FC-41. respectively. RLX could induce very less early apoptosis in the cells due to poor internalization into cells. Notably, drug loaded nanoparticles led to early and late apoptosis induction in within 24 h in MCF-7 cells. Remarkably RLX-FC-41 were capable of inducing higher early and late apoptotic cells percentage than RLX-NH_2-41. It can be concluded that target group played a major role in giving this outcome. Similar pattern was observed for MCM-48 types of nanoparticles as well alongwith 5.61%, 14.63% and 59.11% early apoptosis. (figure 5.39).

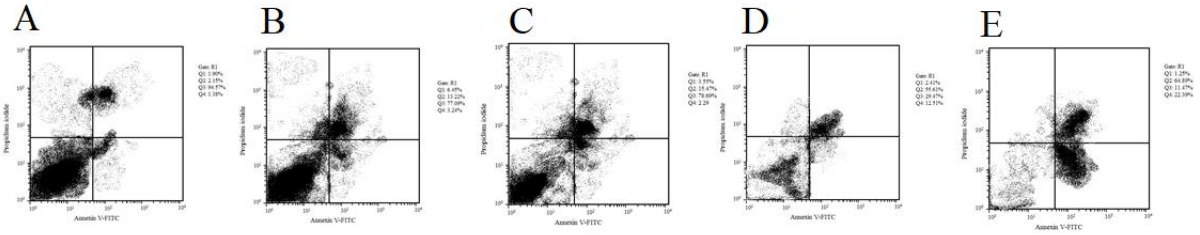

Figure 5.39: apoptosis study for (A) RLX, (B) RLX-NH_2-41, (C) RLX-NH_2-48, (D) RLX-FC-41 and (E) RLX-FC-48

5.3.13. Haemolysis study:

Detailed investigation of heamolysis analysis demonstrated safe nature of formulated nanoparticles. The microscopic analysis for the same is depicted in the figure 5.40. The microscopic image for the RBC treated with Triton X-100 and plain RLX showed ruptured and deformed erythrocyte. Whereas the integrity remained unchanged after treating the RBCs with nanoparticles. Furthermore, the spectral analysis demonstrated 1.98 ± 0.22, 1.56 ± 0.68, 1.15 ± 0.49% and 1.47 ± 0.24% heamolysis RLX-CHITO-41, RLX-CHITO-48, RLX-FC-41 and RLX-FC-48 respectively whereas the value was higher than 5% in case of pure RLX.

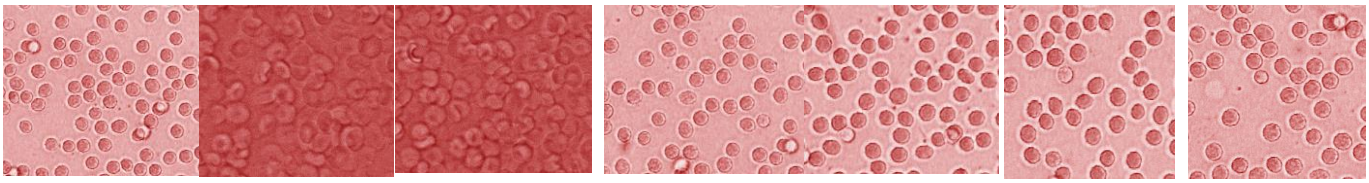

(A) (B) (C) (D) (E) (F) (G)

Figure 5.40: Microscopical and visual images for (A) negative control (B) positive control (C) RLX, (D) RLX-CHITO-41, (E) RLX-CHITO-48, (F) RLX-FC-41 and (G) RLX-FC-48

5.3.14. In vivo pharmacokinetics study for oral formulation:

Poor bioavailability of the RLX is due to limited solubility in water and its extensive first pass metabolism. *In vivo* bioavailability of free RLX and RLX loaded nanoparticles was studied in Swiss albino female mice. Following the sample preparation protocol as mentioned in the earlier section the plasma samples were comprehensively analyzed by optimized and validated RP-HPLC method. Different pharmacokinetic parameters for plain RLX, MF, RLX-41, RLX-48, RLX-NH_2-41 and RLX-NH_2-48 were compared with each other and summarized in the following table 5.11. The pharmacokinetic study outcome revealed significant increment in drug plasma concentration ($p<0.05$) on the administration of formulated nanoparticle in contrast to plain drug. Furthermore, the comparison in the C_{max} value for RLX-41 and RLX-48 divulged higher value of C_{max} for latter nanoparticles. The considerable high plasma concentration after oral administration of RLX-41 and RLX-48 was achieved in 60 min with 5.32 and 5.45 µg/mL plasma concentration compared to 1.25 µg/mL after 1 h for plain RLX. The maximum concentration obtained within 60 min followed by steady fall, which is an indication of the lag period continuing up to 12h. The result gathered here were complementary to the *in vitro* release data wherein the higher RLX release was obtained from RLX-48. Moreover, the lesser C_{max} figure for aminated nanoparticle with respect to bare nanoparticle

could be attributed to hindered RLX release due to the presence of an amine group over the surface. But, the results were still favoring the aminated nanoparticles over plain RLX. Similarly, the $AUC_{(0-24)}$ and $AUC_{(0-infinite)}$ results demonstrated identical pattern of increment as observed for C_{max}. Thus, an overall increment in the bioavailability were 2.11, 3.33, 3.50, 2.27 and 2.55 fold for MF, RLX-41, RLX-48, RLX-NH_2-41 and RLX-NH_2-48 respectively with respect to the RLX pure drug as listed in table 5.11. The significant increase in AUC for RLX nanoparticle could be due the nano size of the formulation and avoidance of the first pass metabolism through the lymphatic transport pathway. The increment in the bioabailability could be attributed to enhanced solubility of RLX in the gastrointestinal tract encapsulating them into MSN framework (figure 5.41).

Table 5.11: Pharmacokinetics parameters for RLX, RLX-41, RLX-48, RLX-NH_2-41 and RLX-NH_2-48

PARAMETERS	RLX	MF	RLX-41	RLX-48	RLX-NH_2-41	RLX-NH_2-48
C_{max} (µg/ml)	1.25 ±0.19	4.02 ±0.11	5.32 ±0.24	5.45±0.35	3.19±0.11	3.53±0.16
$AUC_{(0-24)}$ (µg/ml*h)	10.95 ±0.04	23.07 ±0.12	36.48 ±0.25	38.35±0.44	24.89±0.04	27.97±0.08
$AUC_{(0-infinite)}$ (µg/ml*h)	14.47±0.17	35.39 ±0.07	41.55 ±0.32	44.48±0.23	29.67±0.18	34.43±0.14
$T_{1/2\ (h)}$	5.42 ±0.06	8.29 ±0.06	8.35±0.26	8.47±0.12	4.28±0.05	4.66±0.11
MRT (h)	9.11±0.58	11.33±0.89	11.37±0.55	11.89±0.44	7.52±0.58	7.47±0.47
CL(mg)/(µg/ml)/h	0.86±0.45	0.35±0.27	0.32±0.24	0.28±0.17	0.36±0.84	0.34±0.58
Relative bioavailability	-	2.11	3.33	3.50	2.27	2.55

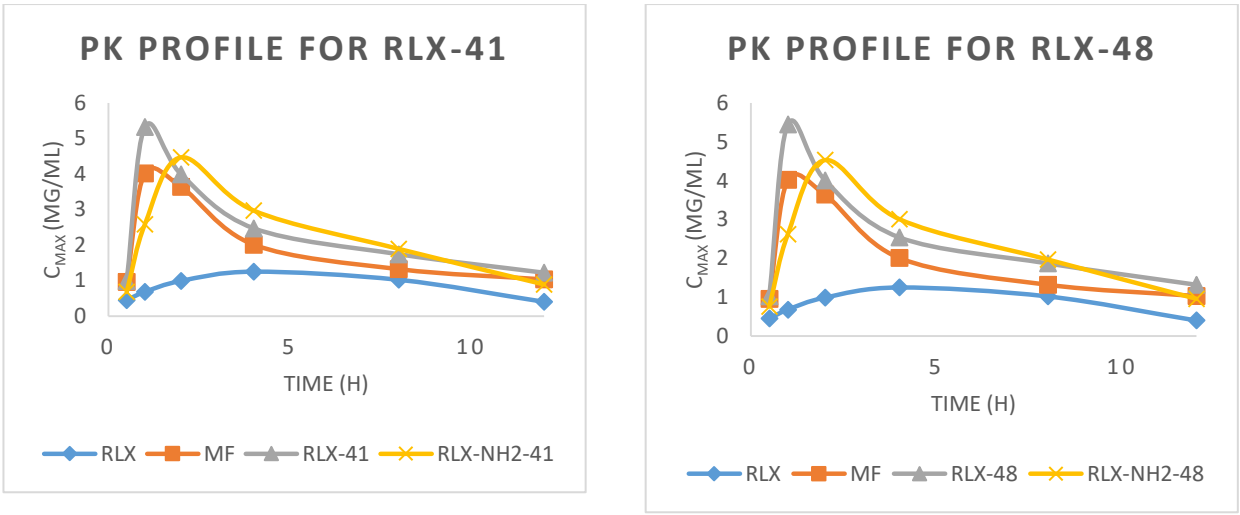

Figure 5.41: *In vivo* pharmacokinetics study for RLX-41 and RLX-48 types nanoparticles

5.3.15 In vivo pharmacokinetics, biodistribution and histological examination study for parenteral formulation:

Statistically significant differences were found in the major pharmacokinetic parameters between RLX and formulations. Free RLX exhibited a more rapid clearance from blood with low $t_{1/2}$ and peak plasma concentration. Whereas, FC coated nanoparticles exhibited a slow and steady clearance with longer $t_{1/2}$ and higher AUC, where higher $t_{1/2}$ indicates the ability of nanocarriers to accumulate at tumor site for a longer time and give enhanced therapeutic effect. The details of pharmacokinetic parameters is summarized in table 5.12 and it is depicted in the figure 5.42

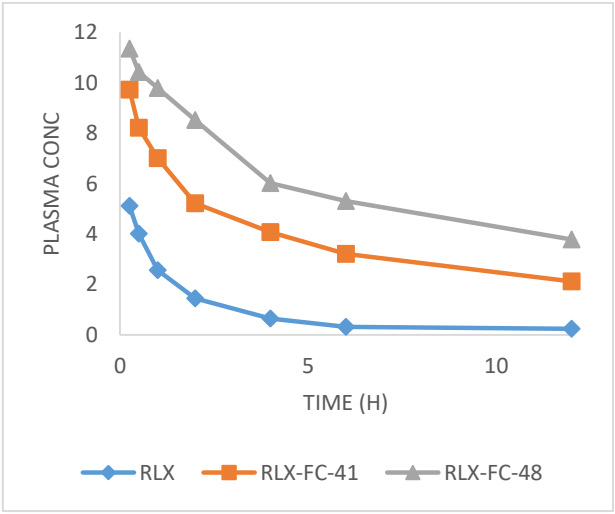

Figure 5.42: *In vivo* pharmacokinetics study for (A) RLX, (B) RLX-FC-41 and (C) RLX-FC-48

Table 5.12: Pharmacokinetics parameters for RLX, RLX-FC-41 and RLX-FC-48

PARAMETERS	RLX	RLX-FC-41	RLX-FC-48
C_{max} (µg/ml)	5.12±0.6	9.72±0.5	11.35±0.1
$AUC_{(0-24)}$ (µg/ml*h)	11.33±01.2	47.35±1.4	72.99±0.9
$T_{1/2\ (h)}$	2.71±0.6	8.82±0.5	12.04±0.8
MRT (h)	3.67±0.7	11.78±0.9	16.39±1.1
Vss (mg)/(µg/ml)	1.51±0.6	0.80±1.3	0.59±1.5
Cl(mg)/(µg/ml)/h	0.41±0.09	0.06±0.02	0.04±0.01

The concentration of RLX in major organs was determined at 24 h. From results it could be inferred that the concentration of RLX-FC-41 and RLX-FC-48 in all major organs were remarkably decreased as compared to RLX alone. Thus, the nanoparticle showed lesser accumulation in all major organs than free drug. This might be due to prolonged blood circulation of MSNs in the bloodstream thus reducing major side effects associated with RLX (figure 5.43).

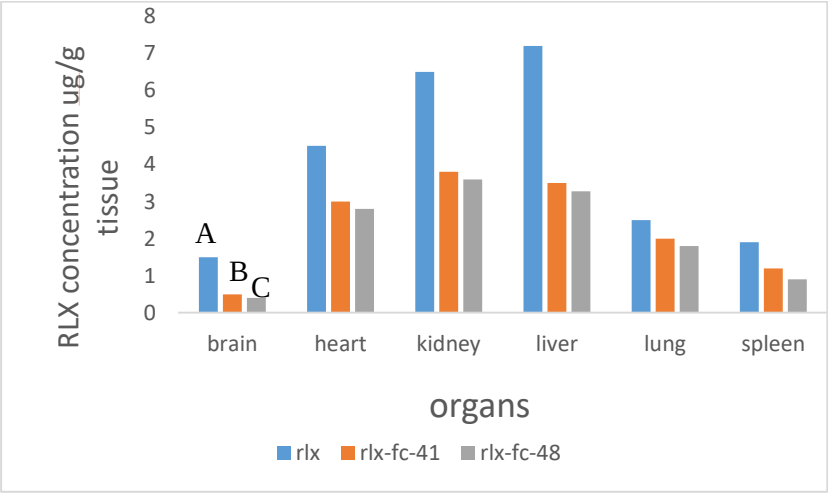

Figure 5.43: Biodistribution graph for (A) RLX, (B) RLX-FC-41 and (C) RLX-FC-48 in different organs

Finally, the histological examination was performed to investigate the safety profile of engineered formulations. The figure 5.44 shows the histological images for plain RLX and RLX loaded nanoparticles. The images revealed no histological evidence of any toxicity in the mice which were given RLX formulation. Thus, it could be concluded that the formulated nanoparticles are safe and not having any toxicity on the major organs.

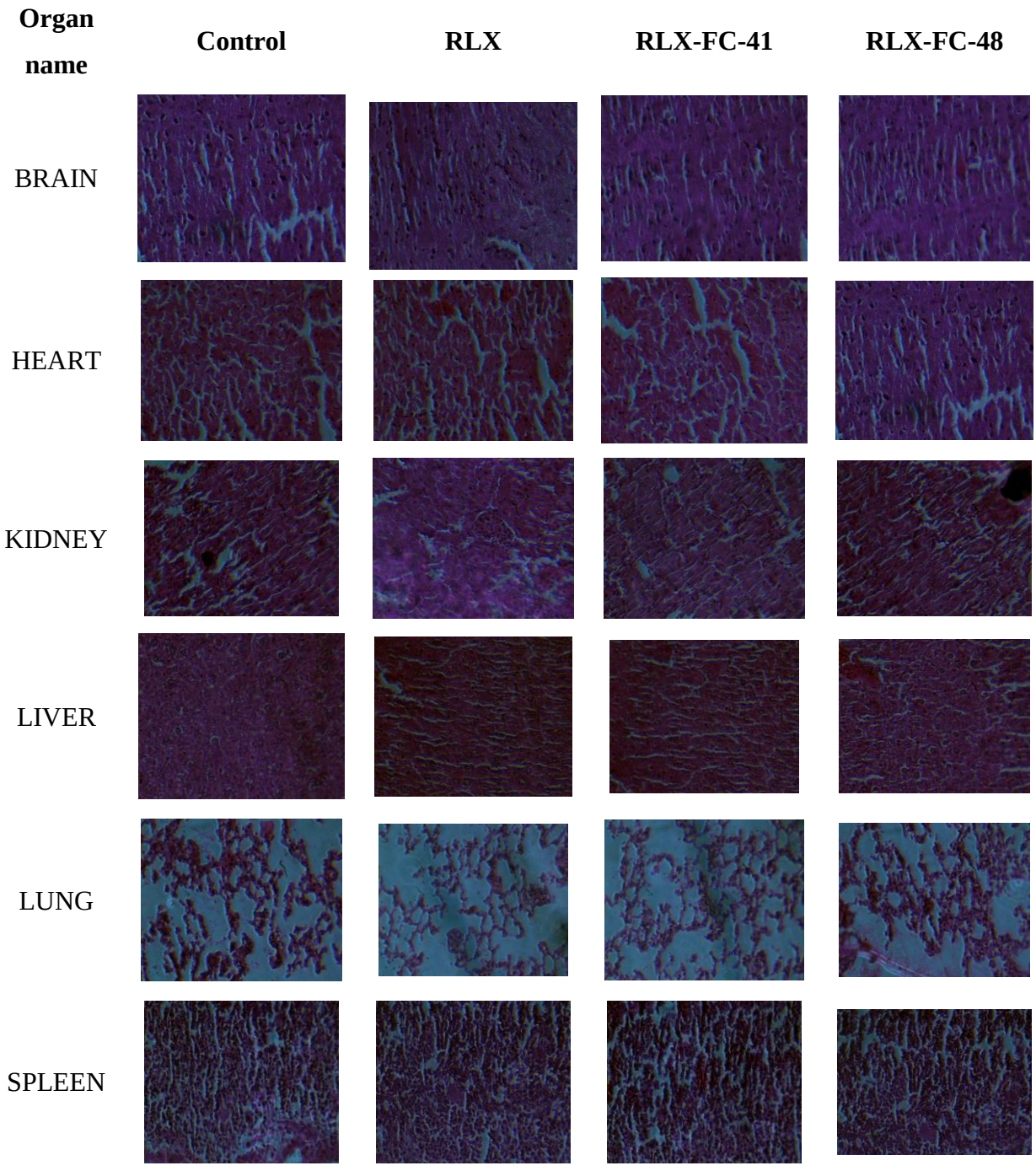

Figure 5.44: Histological images for different formulation given to mice

5.3.16. Stability study of synthesized nanoparticle:

The DSC and SXRD data revealed that the synthesized nanoparticles were stable at 40±2 ºC and 75±5 %RH for the 6 months. The instrumental data revealed identical DSC and SXRD pattern at 0^{th} day and after 6^{th} month as depicted in figure 5.45 and figure 5.46 which strongly supports no degradation or lack of unstability of formulated nanoparticles. In the DSC thermogram of nanoparticles, the peak of RLX was absent which strongly suggest that on

storage there was no leakage of the drug. Furthermore, the identical SXRD pattern at 0th month and after 6th month revealed that the mesoporous skeleton were well preserved.

(A)

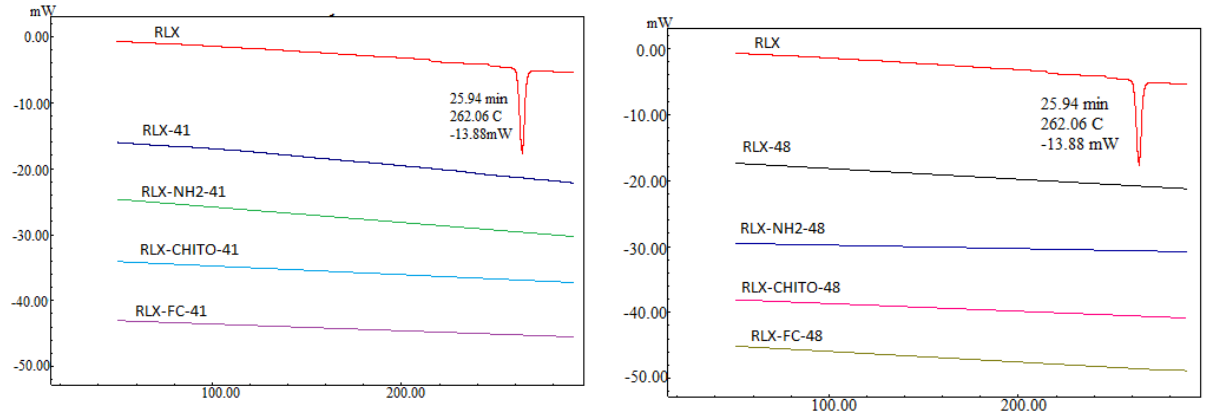

(B)

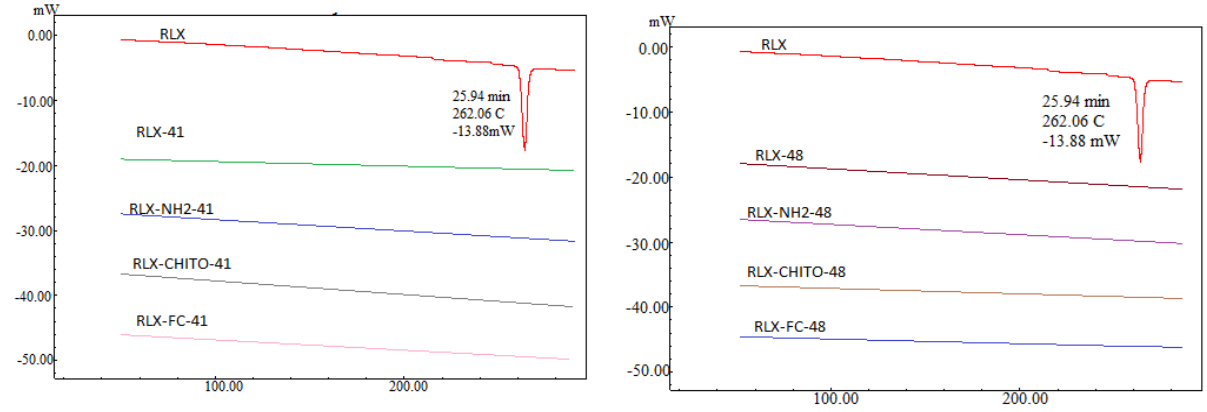

Figure 5.45: DSC thermogram of different nanoparticles at (A) 0th month and (B) 6th month

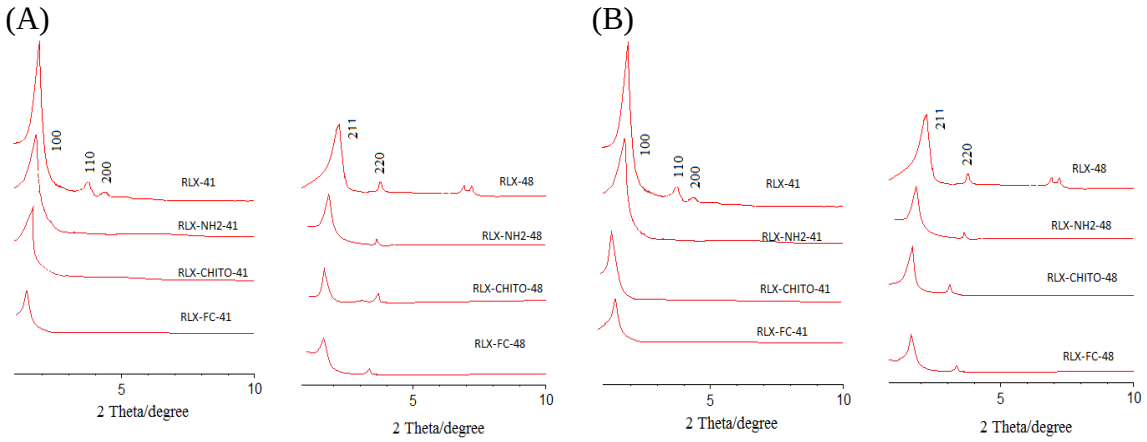

Figure 5.46: SXRD pattern of different nanoparticles at (A) 0th month and (B) 6th month

5.4. Conclusion:

Form the entire study it could be concluded that encapsulation of RLX inside the mesopores of MCM-41 and MCM-48 remarkably improved its drug release profile as well its permeability and thereby the bioavailability was also significantly enhanced. *In vitro* release data exhibited a burst RLX release having a magnitude of 4 and 4.4 times enhancement in the solubility by RLX-41 and RLX-48 with respect to RLX plain drug and 1.2 and 1.6 fold increment respectively in contrast to MF after a one hour of time span. In contrast, though the surface decorated nanoparticle exhibited incomplete RLX release after a period of 300 min, the release were still higher compare to API *i.e.* 2.69 and 2.82 times increment with respect to pure RLX for RLX-NH_2-41 and RLX-NH_2-48 respectively. The *in vitro* permeability data revealed nearly 4.31 and 5.31 fold increment in the permeability for RLX-41 and RLX-48 respectively, whereas the permeability coefficient value was declined for RLX-NH_2-41 and RLX-NH_2-48 with respect to bare nanoparticle but these were still greater as compared to permeability of pure RLX *i.e.* 2.77 and 3.16 respectively. Therefore, the permeability results unveiled enhanced permeability of RLX by designing and encapsulating them into mesoporous nanosystem. The *in vivo* investigation revealed an overall 3.33, 3.50, 2.77 and 2.55 fold increment in the bioavailability for RLX-41, RLX-48, RLX-NH_2-41 and RLX-NH_2-48.with respect to the RLX pure drug. The increment in the bioabailability could be attributed to enhanced solubility of RLX in the gastrointestinal tract encapsulating them into MSN framework. Additionally, the cellular uptake study for chitosan coated nanoparticles and folate attached nanoparticles evidenced higher uptake of surface functionalized nanoparticles compared to bare nanoparticles. This investigation unveiled 2.1, 2.8, 2.3 and 3.3 times increment in cellular uptake for MCM-CHITO-41, MCM-FC-41, MCM-CHITO-48 and MCM-FC-48 respectively as compared to pristine nanoparticles. This could be helpful in directing the drug release to cancer cells only and thereby also help in dose reduction as well as its adverse effect to healthy cells as the amount reaching to non-tumor cells would be decreased by surface coating. Lastly, the histological examination and biodistribution study demonstrated safe nature of engineered nanoaprticles.

5.5. References:

1. Jordan V. Beyond raloxifene for the prevention of osteoporosis and breast cancer. British journal of pharmacology. 2007;150(1):3-4.

2. Ettinger B, Black DM, Mitlak BH, Knickerbocker RK, Nickelsen T, Genant HK, et al. Reduction of vertebral fracture risk in postmenopausal women with osteoporosis treated with raloxifene: results from a 3-year randomized clinical trial. Jama. 1999;282(7):637-45.

3. Shah N, Seth A, Balaraman R, Sailor G, Javia A, Gohil D. Oral bioavailability enhancement of raloxifene by developing microemulsion using D-optimal mixture design: Optimization and in-vivo pharmacokinetic study. Drug development and industrial pharmacy. 2017:1-10.

4. Patil PH, Belgamwar VS, Patil PR, Surana SJ. Solubility enhancement of raloxifene using inclusion complexes and cogrinding method. Journal of pharmaceutics. 2013;2013.

5. Shah NV, Seth AK, Balaraman R, Aundhia CJ, Maheshwari RA, Parmar GR. Nanostructured lipid carriers for oral bioavailability enhancement of raloxifene: design and in vivo study. Journal of advanced research. 2016;7(3):423-34.

6. Shah PV, Rajput SJ. Facile Synthesis of Chitosan Capped Mesoporous Silica Nanoparticles: A pH Responsive Smart Delivery Platform for Raloxifene Hydrochloride. AAPS PharmSciTech. 2018:1-14.

7. Gulfam M, Chung BG. Development of pH-responsive chitosan-coated mesoporous silica nanoparticles. Macromolecular Research. 2014;22(4):412-7.

8. Rampino A, Borgogna M, Blasi P, Bellich B, Cesàro A. Chitosan nanoparticles: preparation, size evolution and stability. International journal of pharmaceutics. 2013;455(1-2):219-28.

9. Woraphatphadung T, Sajomsang W, Gonil P, Treetong A, Akkaramongkolporn P, Ngawhirunpat T, et al. pH-Responsive polymeric micelles based on amphiphilic chitosan derivatives: Effect of hydrophobic cores on oral meloxicam delivery. International journal of pharmaceutics. 2016;497(1-2):150-60.

10. Daryasari MP, Akhgar MR, Mamashli F, Bigdeli B, Khoobi M. Chitosan-folate coated mesoporous silica nanoparticles as a smart and pH-sensitive system for curcumin delivery. Rsc Advances. 2016;6(107):105578-88.

11. Wouters BH, Chen T, Dewilde M, Grobet PJ. Reactivity of the surface hydroxyl groups of MCM-41 towards silylation with trimethylchlorosilane. Microporous and mesoporous materials. 2001;44:453-7.

12. Xu J, Luan Z, He H, Zhou W, Kevan L. A reliable synthesis of cubic mesoporous MCM-48 molecular sieve. Chemistry of materials. 1998;10(11):3690-8.

13. Ebrahimi-Gatkash M, Younesi H, Shahbazi A, Heidari A. Amino-functionalized mesoporous MCM-41 silica as an efficient adsorbent for water treatment: batch and fixed-bed column adsorption of the nitrate anion. Applied Water Science. 2015:1-15.

14. Yoncheva K, Popova M, Szegedi A, Mihály J, Tzankov B, Lambov N, et al. Functionalized mesoporous silica nanoparticles for oral delivery of budesonide. Journal of Solid State Chemistry. 2014;211:154-61.

15. Shah PV, Rajput SJ. A comparative in vitro release study of raloxifene encapsulated ordered MCM-41 and MCM-48 nanoparticles: A dissolution kinetics study in simulated and biorelevant media. Journal of Drug Delivery Science and Technology. 2017;41:31-44.

16. Rosen JE, Gu FX. Surface functionalization of silica nanoparticles with cysteine: a low-fouling zwitterionic surface. Langmuir. 2011;27(17):10507-13.

17. Ding Y, Shen SZ, Sun H, Sun K, Liu F, Qi Y, et al. Design and construction of polymerized-chitosan coated Fe 3 O 4 magnetic nanoparticles and its application for hydrophobic drug delivery. Materials Science and Engineering: C. 2015;48:487-98.

18. de Oliveira LFa, Bouchmella K, Gonçalves KdA, Bettini J, Kobarg Jr, Cardoso MB. Functionalized silica nanoparticles as an alternative platform for targeted drug-delivery of water insoluble drugs. Langmuir. 2016;32(13):3217-25.

19. Saroj S, Rajput SJ. Etoposide encapsulated functionalized mesoporous silica nanoparticles: Synthesis, characterization and effect of functionalization on dissolution kinetics in simulated and biorelevant media. Journal of Drug Delivery Science and Technology. 2017.

20. Lu H-T. Synthesis and characterization of amino-functionalized silica nanoparticles. Colloid Journal. 2013;75(3):311-8.

21. Deng L, Wang Y, Gong T, Sun X, Zhang Z-R. Dissolution and bioavailability enhancement of alpha-asarone by solid dispersions via oral administration. Drug development and industrial pharmacy. 2017;43(11):1817-26.

22. Marques M. Dissolution media simulating fasted and fed states. Dissolution Technologies. 2004;11(2):16-9.

23. Klein S. The use of biorelevant dissolution media to forecast the in vivo performance of a drug. The AAPS journal. 2010;12(3):397-406.

24. Salis A, Fanti M, Medda L, Nairi V, Cugia F, Piludu M, et al. Mesoporous silica nanoparticles functionalized with hyaluronic acid and chitosan biopolymers. Effect of

functionalization on cell internalization. ACS Biomaterials Science & Engineering. 2016;2(5):741-51.

25. Huo J, Aguilera-Sigalat J, El-Hankari S, Bradshaw D. Magnetic MOF microreactors for recyclable size-selective biocatalysis. Chemical science. 2015;6(3):1938-43.

26. Senthilkumar R, Karaman DŞ, Paul P, Björk EM, Odén M, Eriksson JE, et al. Targeted delivery of a novel anticancer compound anisomelic acid using chitosan-coated porous silica nanorods for enhancing the apoptotic effect. Biomaterials science. 2015;3(1):103-11.

27. Zhao Y, Sun X, Zhang G, Trewyn BG, Slowing II, Lin VS-Y. Interaction of mesoporous silica nanoparticles with human red blood cell membranes: size and surface effects. ACS nano. 2011;5(2):1366-75.

28. Akrami M, Khoobi M, Khalilvand-Sedagheh M, Haririan I, Bahador A, Faramarzi MA, et al. Evaluation of multilayer coated magnetic nanoparticles as biocompatible curcumin delivery platforms for breast cancer treatment. RSC Advances. 2015;5(107):88096-107.

29. Li J, Zheng L, Cai H, Sun W, Shen M, Zhang G, et al. Polyethyleneimine-mediated synthesis of folic acid-targeted iron oxide nanoparticles for in vivo tumor MR imaging. Biomaterials. 2013;34(33):8382-92.

30. Heikkilä T, Salonen J, Tuura J, Hamdy M, Mul G, Kumar N, et al. Mesoporous silica material TUD-1 as a drug delivery system. International journal of pharmaceutics. 2007;331(1):133-8.

31. Zhang Y, Zhi Z, Jiang T, Zhang J, Wang Z, Wang S. Spherical mesoporous silica nanoparticles for loading and release of the poorly water-soluble drug telmisartan. Journal of Controlled Release. 2010;145(3):257-63.

32. Kim JM, Chang SM, Kong SM, Kim K-S, Kim J, Kim W-S. Control of hydroxyl group content in silica particle synthesized by the sol-precipitation process. Ceramics International. 2009;35(3):1015-9.

33. de Oliveira Freitas LB, Bravo IJG, de Almeida Macedo WA, de Sousa EMB. Mesoporous silica materials functionalized with folic acid: preparation, characterization and release profile study with methotrexate. Journal of Sol-Gel Science and Technology. 2016;77(1):186-204.